# UC Santa Barbara

**UC Santa Barbara Electronic Theses and Dissertations**

**Title**

Kinetic Isotope Effect in the Excited State Intramolecular Proton Transfer in Isolated Jet-Cooled Indigo Dye

**Permalink**

https://escholarship.org/uc/item/2ss041qd

**Author**

Vo, Krystal

**Publication Date**

2022

Peer reviewed|Thesis/dissertation

UNIVERSITY OF CALIFORNIA

Santa Barbara

Kinetic Isotope Effect in the Excited State Intramolecular Proton Transfer in

Isolated Jet-Cooled Indigo Dye

A Thesis submitted in partial satisfaction of the

requirements for the degree Master of Science

in Chemistry

by

Krystal Thanh Vo

Committee in charge:

Professor Mattanjah S. De Vries, Chair

Professor Joan-Emma Shea

Professor Steven K. Burratto

September 2022

The thesis of Krystal Thanh Vo is approved.

_____

Joan-Emma Shea

_____

Steven K. Burratto

_____

Mattanjah S. de Vries, Committee Chair

September 2022

Kinetic Isotope Effect in the Excited State Intramolecular Proton Transfer in

Isolated Jet-Cooled Indigo Dye

ACKNOWLEDGEMENTS

## *Curriculum Vitae* of **Krystal Thanh Vo**

September 2022

Department of Chemistry and Biochemistry
University of California, Santa Barbara, CA 93106
Citizenship: U.S.A.
ktvo@ucsb.edu          vokrystal@gmail.com
805-893-4720 (lab)          404-457-6463 (cell)

## EDUCATION

| 2019 – 2022 | **Master of Science (M.S.)** | Physical/Analytical Chemistry<br>University of California, Santa Barbara<br>Advisor: Prof. Mattanjah S. de Vries |
| --- | --- | --- |
| 2012 - 2015 | **Bachelor of Science (B.S.)** | Chemistry<br>University of Georgia, Athens |

## RESEARCH EXPERIENCE

**Graduate Student**, UC Santa Barbara, 2019 – 2022
Advisor: Prof. Mattanjah S. de Vries

Investigated the photochemical relaxation mechanism of isolated internally cooled molecules by applying laser desorption, molecular beams, resonance enhance multiphoton ionization techniques (REMPI), and time of flight mass spectrometry (TOF-MS) for high electronic and vibrational resolution experiments. Performed pump probe experiments to measure excited state lifetimes. Utilized high vacuum systems including diffusion pumps, laser maintenance, operation, and troubleshooting lasers (Nd:YAG, optical parametric generator OPG), LabVIEW software, Mathematica, oscilloscopes, delay/pulse generators, laser alignment tools, optics, harmonic generation

**Laboratory Assistant,** Ray Biotech (Lilburn, GA) 2018 – 2019

Assisted with the development of new proteomic tools such antibody, protein, glycobiology, phosphorylation, peptide mapping, and multiplex protein arrays.

**Analytical R&D Chemist**, Biolab, KIK Custom Products (Lawrenceville, GA) 2015 – 2018

Developed methods for the innovation of new consumer chemical products such as pool chemicals, household cleaning, and sun care products. Operated gas chromatography flame ionization detection (GC-FID), high performance liquid chromatography (HPLC) (LCMS), inductive coupled plasma optical emission spectroscopy (ICP-OES), thermogravimetric analysis (TGA), differential scanning calorimetry (DSC), FT-IR, UV-VIS, and wet chemistry analysis such as potentiometric titrations. Regulatory experience includes EPA Good Laboratory Practices (GLP), development of standard operating procedures (SOPs), and FDA Current Good Manufacturing Practice (cGMP)

**Undergraduate Research Assistant,** University of Georgia (UGA), Athens 2013 – 2014
Advisor: Prof. Shanta Dhar

    Assisted in the study of nanotechnology-based drug delivery systems in targeting cancer cells. Employed cell culturing techniques, polymer synthesis and analysis, diffractive light scattering analysis (DLS), gel permeation chromatography (GPR), and NMR

**Undergraduate Research Assistant,** UGA Complex Carbohydrate Research Center
(Athens, GA) 2014 – 2015
Advisor: Prof. Lianchun Wang

    Assisted in the study of heparan sulfate proteoglycan and its role in vascular development. Used gene knockout techniques, real time cell proliferation studies, mouse study, genotyping, gel electrophoresis, and PCR to elucidate the underlying cellular and molecular mechanisms of expression at cell surfaces

## TEACHING EXPERIENCE

**Teaching Assistant**, UC Santa Barbara (2019 - 2022)
- Taught undergraduate laboratory courses: general chemistry laboratory, organic chemistry laboratory, advance inorganic synthesis physical chemistry laboratory
- Taught undergraduate lectures: analytical chemistry, environmental chemistry, and photochemistry and radiation

**STEM Tutor**, Georgia State University (2015 – 2017)

## HONORS AND AWARDS

- UCSB Grand Slam Final Round Participant (2022) *Photochemistry of Pigments*
- UCSB Outstanding Service to the Department Award (2022)
- Jarrod Davidson Memorial Scholarship Recipient (2021)
- Georgia HOPE Scholarship Recipient (2012 – 2015)
- Zell Miller Scholarship Recipient (2012 - 2015)

## PRESENTATIONS

1. Oral Presentation: 2021 29th International Symposium on Molecular Beams
   *UV Photodynamics of Thymine-Thymine Stacked Nucleobases in Peptide Nucleic Acids*
2. Poster Presentation: 2022 ACS Spring National Conference, *When an excited indi-goes fast*
3. Poster Presentation: 2022 Origins of Life Gordon Research Seminar: *UV Photodynamics of Thymine-Thymine Stacked Nucleobases in Peptide Nucleic Acids*
4. Poster Presentation: 2021 International Symposium on Molecular Beams Conference: *Proton Transfer and Hydrogen Transfer in Photorelaxation of Indigo*

ABSTRACT


Kinetic Isotope Effect in the Excited State Intramolecular Proton Transfer in

Isolated Jet-Cooled Indigo Dye


by


Krystal Thanh Vo

Excited state intramolecular proton transfer (ESIPT). To elucidate the mechanism of ESIPT and reaction barrier of tunneling mechanism in indigo, a combination of laser desorption, jet cooling, resonance enhanced multiphoton ionization (REMPI), time-of-flight mass spectrometry is employed to produce vibronically resolved spectra of deuterium substituted indigo. The picosecond two color REMPI spectrum of indigo displayed a red shift and peak splitting upon deuterium substitution on and above the barrier, as well as no shift or blue shift below the barrier, where the barrier corresponds to the separation of the proton transfer and hydrogen transfer forms of the keto-enol tautomer in the S1 state. In pump probe measurements, deuterium substitution induces a longer excited state lifetime with a $k_h/k_d$ ratio of 2.5, indicating that tunnel effect takes place in the ESIPT of the non-deuterated system.

# TABLE OF CONTENTS

# I. Introduction

### A. *Unraveling the Mechanism Behind Excited State Intramolecular Proton Transfer*

Excited state intramolecular proton transfer (ESIPT) forms the basis of many important biological and chemical processes, but the physical chemistry of the reaction is still not fully understood. It was proposed by Weller who observed a dual fluorescence in methyl salicylate attributing to a three-energy level system in containing the ground state, a normal excited state, and a tautomer excited state [1]. ESIPT has since attracted attention in a plethora of applications such as lasers [2], fluorescent molecular probes [3], white light-emitting materials [4] [5], and optical devices [6]. When a molecule with a suitable chromophore absorbs a photon and undergoes a $\pi$-$\pi^*$ transition to the $S_1$ state, it can experience a redistribution of electronic charge in which the proton donating and accepting groups increase in acidity and basicity, respectively, in the excited state. One can describe the proton as wanting to "catch up" with a new electron distribution in the excited state. Two delocalized n-electrons become localized on the two carbon atoms which bear the groups forming the intramolecular hydrogen bond. In many systems investigated, the proton is transferred along the hydrogen bond between from the nitrogen atom to oxygen. This process is ultrafast and occurs in the order of femtoseconds [7]. Following ESIPT are significant changes in dipole moments and molecular geometry, resulting in strongly Stokes-shifted fluorescence of the tautomer in which the formation can range from the femtosecond to microsecond time domain depending on the system [8]. Relaxation may be radiative or non-radiative, but in either cases usually involve reverse isomerization or back proton transfer to the ground state. It is also important to consider the distinction between excited

state proton transfer and hydrogen transfer, both of which involves tautomerization. It was first proposed that in proton transfer, the zwitterionic tautomer is formed whereas in hydrogen transfer, a keto tautomer is formed as opposed to the enol form in the ground state. The fundamental difference is the distribution of electron density, where only the proton moves in proton transfer and the electron is translocated synchronously with the proton in hydrogen transfer. For the keto tautomer to be stabilized in hydrogen transfer, internal electronic and nuclear rearrangements must take place [9]. It is not to confuse with proton coupled electron transfer, in which proton transfer and electron transfer occur stepwise. Hence, it is important to understand the charge redistribution along the reaction path to properly describe the reaction, as the differences in dynamics and relaxation pathways of the tautomer could be used as a tool in spectroscopy.

ESIPT can be solvent assisted and called pseudo-intramolecular. Gas phase studies will be discussed to investigate the intrinsic molecular properties unencumbered by environmental couplings that obscure the true dynamics of the natural phenomenon. ESIPT mechanism varies by systems and may occur by thermal and/or photoinduced activation, in a barrierless process or through a barrier, which is referred as quantum mechanical proton tunneling. Unlike classical particles that must go over energy barrier, hydrogen can be described as a wave packet and can therefore penetrate through potential energy barrier. This implies that the nucleus may pass from reactants to products, remaining below the top of the barrier because the mass of a hydrogen (or deuterium) is small enough that it is not necessary for the particle to climb over the barrier [10]. The rate of tunneling is dependent on deuterium isotope effect, vibrational excess energy, dependence on barrier height and width. Substitution of the hydrogen for a deuterium isotope is a method for probing the barrier on a

potential energy surface (PES) as tunneling is sensitive to mass effects. The rate of the two-dimensional tunneling model through a double minimum potential barrier (for hydrogen $H$ or deuterium $D$) can be described by the following equation given by Bell [11]:

$$k_{H.D} = v_{H.D}^{-(\frac{\pi a_0}{\hbar})(2mU_0)^{1/2}}$$

Eq (1)

where $v_{H.D}$ is the O-H vibrational frequency, $m$ is the effective mass, $a_0$ is the barrier half width, and $U_0$ is the barrier height [12] [13]. Hence, deuteration can reduce the transfer rate by reducing frequency $v$, doubling the effective mass $m$, and reducing the zero-point energy by a factor of $\sqrt{2}$. The equation can be rearranged to obtain the effect of deuterium substitution on proton tunneling:

$$\frac{k_h}{k_d} = (\frac{v_h}{v_d})^{0.38 a_0 \sqrt{v_0}(\sqrt{\mu_d} - \sqrt{\mu_h})}$$

Eq (2)

where $a_0$ is in angstroms, $v_0$ is in cm$^{-1}$, and u is $m_1 m_2 / (m_1 + m_2)$ in Daltons. In the case of tunneling, the probability will increase with an increase in $k_h/k_d$ since the probability for hydrogen to tunnel is greater than deuterium. In the two-dimensional model, the PES minima may be symmetric with a high energy barrier or asymmetric with a low energy barrier as an exit channel to non-radiative transition. Several studies have studied ESIPT using deuterium substitution of the hydrogen atom to investigate the two-dimensional tunneling model by comparing proton and deuteron transfers. Vibronically resolved spectroscopic studies in absence of solvent observed splitting in the spectra in symmetric hydrogen transfer molecules due to hydrogen atom tunneling on sub picosecond time scales, with the splitting being sensitive to the degree of deuteration [14].

Time resolved spectroscopy of kinetic isotope effects in conjunction with theoretical calculations can elucidate information on PES and barrier. Strandjord et al. demonstrated

that the proton-transfer process has a fast and a slow kinetic component in 3-hydroxyflavone [15]. To elucidate tunneling and mass effects on the excited potential surface, real-time probing of methyl salicylate (MS) under collision-less conditions tested deuterium substitution effects on ESIPT [16]. A delayed femtosecond pulse depleted the initial enol and final keto tautomer populations, probing the PES of the internal H-atom motion, which was observed to take place within 60 femtoseconds. Isotope effects were not observed in deuterium substitution of MS, indicating a barrierless reaction and hence, absence of tunneling. In a study on jet-cooled isolated 2-(2'-hydroxyphenyl)-5-phenyloxazole (HPPO) and deuterated form, deuteration resulted in drastic narrowing of fluorescence bands and decrease in rate constant [17]. This deuteration effect is a signature of the tunneling mechanism and the existence of two PES minima. In addition, it was determined that the PES was largely asymmetric due to the absence of any resonant fluorescence from the enol form and a blue shift in the excitation spectrum. The rate constant was determined with the full width at half maximum (FWHM) intensity of the vibronic band expressed as:

$$\text{FWHM} = \frac{1}{2\pi c\tau} \qquad \text{Eq (3)}$$

where $c$ is the speed of light and $\tau$ is lifetime of a given vibronic state of the isolated molecule. The upper limit of the rate constant of ESIPT reaction of the main vibronic bands in the excitation spectra could be determined by:

$$k_{\text{ESIPT}} = \frac{1}{\tau} \qquad \text{Eq (4)}$$

resulting in a significantly reduced rate constant (about six times smaller) for the deuterated form, indicating a tunneling mechanism. The energy barrier height was calculated for deuterated and non-deuterated HPPO using $k_{\text{ESIPT}}$ in a mono-dimensional simplified model,

4

which provided a lower energy barrier height in the deuterated form. This contradicts Bell's rate constant given in equation 1, which would predict a higher energy barrier height and width in deuterated HPPO due to an increased mass and induced change in zero-point energies. In another study of jet-cooled isolated 1-hydroxy-2-acetonaphthone (HAN) which exhibits a dual fluorescence character with a double PES minimum in the ground state and an asymmetric double well PES in the excited state. [18] Interestingly, deuteration of HAN completely eliminates the short wavelength part of the fluorescence emission (enol fluorescence) while the long wavelength part (keto fluorescence) remains unchanged, establishing the presence of tunneling through a small energy barrier. This may be due to a large intramolecular electronic redistribution leading to ESIPT. In agreement with Bell's tunneling rate constant equation, it was observed that the lifetime for deuterated HAN (13ns) was longer than the non-deuterated form (9.4ns). These contrasting results highlight the opportunity isolated gas phase studies provide in elucidating tunneling effects in ESIPT dynamics and the complexity in contrasting mechanisms.

### B. Investigation of Excited State Intramolecular Proton Transfer in Indigo Dye

Hydrogen bonding is fundamental in biology and chemistry. However, the role of hydrogen bonding in energy deactivation is not fully understood. Indigo is an organic blue dye that has been used for centuries due to its longevity, which is contributed by its two intramolecular hydrogen bonds between the two adjacent pairs of carbonyl and NH groups owing intrinsic photo-stabilizing mechanism: excited state intramolecular proton transfer (ESIPT). Indigo can serve as a model to elucidate energy dissipation via rapid radiation-less deactivation channel for complex hydrogen bonding systems. Due to its intrinsic

5

photochemical properties, it has been used in a variety of applications such as textiles (blue jeans), transistors [19], solar cells [20], diodes [21], memory storage [22], biosensors [23], and more [24]. A thorough computational study by Yamazaki et al. describes the molecular mechanisms of the photostability of indigo. When indigo is irradiated with light and absorbs a photon, it goes from the ground state $S_0$ to the excited electronic state singlet $S_1$ in a $\pi$-$\pi^*$ transition. ESIPT in indigo occurs when the hydrogen atom is transferred from the nitrogen atom of the amine group to the oxygen atom of the carbonyl group, exhibiting a single proton transfer. When both hydrogen atoms are transferred on both nitrogen groups to oxygen groups, this is double proton transfer. Double proton transfer, along with photoisomerization, are excited state deactivation channels with high reaction barriers and are not discussed here [25]. The intrinsic photostability of indigo is due to the tautomerization from the di-keto to mono-enol form during ESIPT after irradiation and occurs in the femtosecond timescale. Following ESIPT, there is a fast non-radiative decay on the $S_1$ PES minimum with a planar conical intersection to the $S_0$ states that involves deformation of the aromatic rings, providing an internal conversion pathway [25; 26]. Therefore, the keto conformation can be observed when the molecule returns to the ground state in the picosecond timescale. The fast non-radiative decay may be due to tunneling effects, which has been investigated by deuterium substitution effects to obtain an understanding of the reaction barrier.
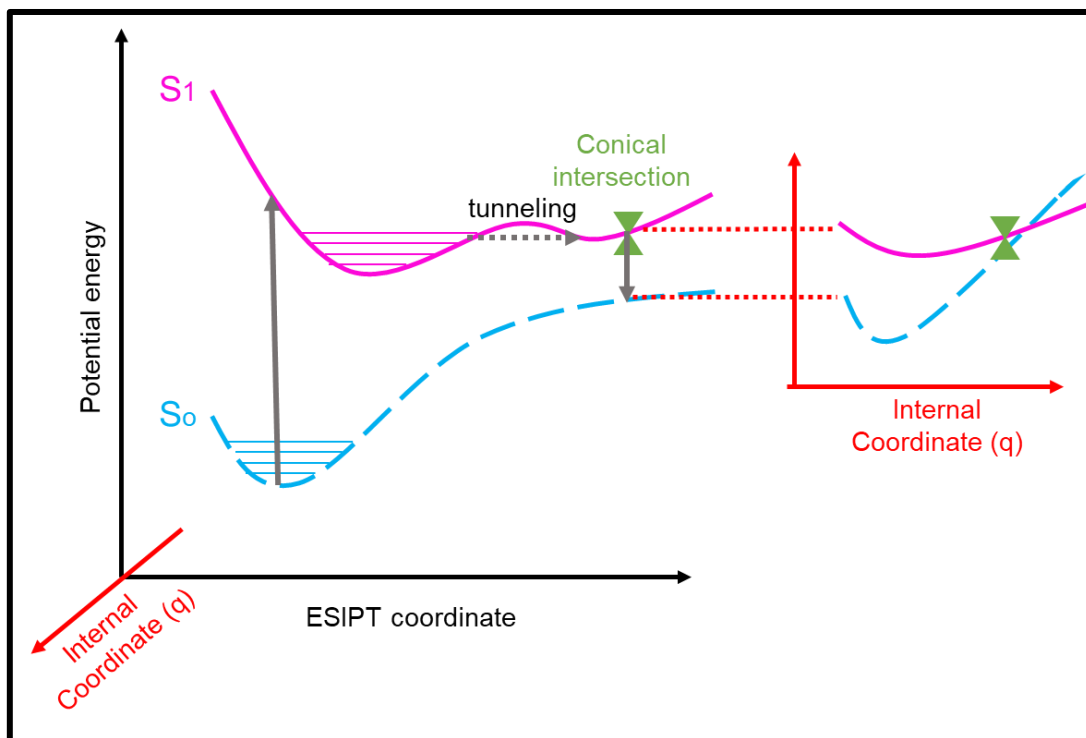
**Figure 1. Diagram representing the potential-energy profile of the SPT tunneling reaction of indigo connecting the $S_1$ minimum with conical intersection (CI).**

An ultrafast femtosecond study by Izumi et al. investigating the ESIPT of indigo carmine provided direct evidence that single proton transfer is a stepwise pathway resulting in a mono-enol structure, ultrafast return to the keto structure, and a back reaction in the order of picoseconds, all of which provide photostability. Following photoexcitation the stretching modes of the two identical carbonyl groups ($v_{C=O}$) were observed. The electron density in one of these acceptor groups in the first proton transfer decreases by $\pi$-electron delocalization extending to the transferred proton. This results in the red shift of $v_{C=O}$. The electron density increases in the C-O bond that does not participate in PT by loss of intramolecular hydrogen bonding between N–H and C=O, resulting in a blue shift of $v_{C=O}$ [27]. Several groups have studied the ESIPT reaction barrier and tunneling mechanism in indigo and substituted indigo derivatives by the deuterium substitution method. Table 1  in

appendix summarizes the results of kinetic isotope studies discussed in this section. In a pump probe femtosecond transient absorption spectroscopy experiment by Nagasawa et al., indigo carmine was deuterated, resulting in a recovery signal ten times slower than the undetuerated form and suggesting the influence of hydrogen bonding in the ultrafast deactivation process [28]. In a study by de Melo et al. on deuterated indigo and its derivatives with di-, tetra-, and hexa-substitution displayed a threefold increase in the fluorescence quantum yield upon deuteration, supporting the idea that proton transfer plays a crucial role in the radiation-less internal conversion pathway and that radiation-less process dominates over radiative rate process. Substitution did not affect highly efficient internal conversion and the decay was observed to be biexponential, indicating two excited species exist: the keto and enol form of indigo [29]. In another study by de Melo et al. the rate constant was probed on the picosecond timescale and observed to be $8.4 \times 10^{10}$ s$^{-1}$ for indigo and $1.6 \times 10^{11}$ s$^{-1}$ for deuterated indigo in a non-polar aprotic solvent, with a $k_H/k_D$ ratio of 0.53. The $k_H/k_D$ ratio of less than 1 is a consequence of the reverse isotope effect. In the reverse isotope effect, the PES for the heavier atom is smaller because the force constant at the transition state (the enol form) becomes larger than that in the initial state (keto form). In this case, the force constant for the enol form is 1006 kcal/(mol Å$^2$) for the O-H bond and 914 kcal/(mol Å$^2$) for the N-H bond [30]. This reversal in trend is typically the case for ionic bonds where the bridging hydrogen is weakened when replaced by deuterium, as opposed to strengthened in pair of neutral molecules. Note that the energy of the system is not changed, but the zero point energy for the heavier atom is reduced [10].
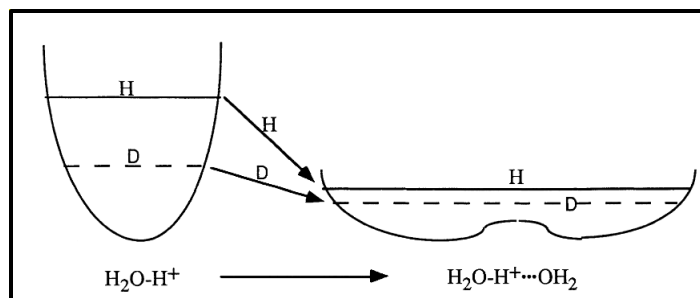
**Figure 2. Zero-point vibrational levels for H and D in the case of an isolated species, on the left, and an ionic H-bond on the right, observed in a reversal trend [10].**

In another femtosecond study by Iwakura et al., kinetic isotope effects were investigated in indigodisulfonate salt in solution and observed a red shift for the C=O stretching mode in deuterated form. $k_d$ was observed to be 2 x $10^{12}$ s$^{-1}$ and 3 x $10^{12}$ s$^{-1}$ for $k_h$ with a $k_h/k_d$ ratio of 1.7 indicating that tunneling takes place in proton transfer [31]. Iwakura et al. also investigated indigo carmine in solution in femtosecond experiments and similarly observed kh to be 3 x $10^{12}$ s$^{-1}$ and kd to be 2 x $10^{12}$ s$^{-1}$ with a $k_h/k_d$ ratio of 1.5 in the early transition state, corresponding to a 44% decrease in deuterated rate constant. A red shift for the C=O stretching mode in deuterated form was also observed in early transition, followed by a blue shift and then a red shift again. This oscillatory feature was not observed in the non-deuterated form as the proton transfer rate is much faster than molecular vibrations. The transition state of the recovery process is faster than the transition state of mono-alcohol generation, which may be attributed to the instability and higher activation energy of the mono-alcohol form [32]. Huber et al. also observed an increase in fluorescence quantum yield in various indigo derivatives and increased cis-trans photoisomerization, a high barrier relaxation pathway, in deuterated indigo in solvent due to reduction/elimination of ESIPT [33]. In a femtosecond study by Roy et al., differences in kinetic isotope effects for indigo carmine were observed between protic and aprotic solvents in which excited state decay

upon deuteration was faster in protic solvents than in aprotic solvents. This may be attributed to significant changes in dipole moment in protic solvents in which intermolecular hydrogen bonds influences the rapid nonradiative $S_1 \rightarrow S_0$ transition via the mono-enol intermediate [34]. Most notably within our research group, Haggmark et al. mapped ESIPT relaxation pathway of isolated indigo in a molecular beam using resonance enhance multiphoton ionization (REMPI), allowing for probing excited state lifetimes of vibronic bands using pump probe spectroscopy in the picosecond and nanosecond range [35]. Two excited state lifetimes at lower excitation energies of the mono-enol intermediate deactivation channels were observed in the order of one and ten nanosecond (ns) timescale. In the higher excitation energies, the longer-lived lifetime was absent as seen in Figure 3.
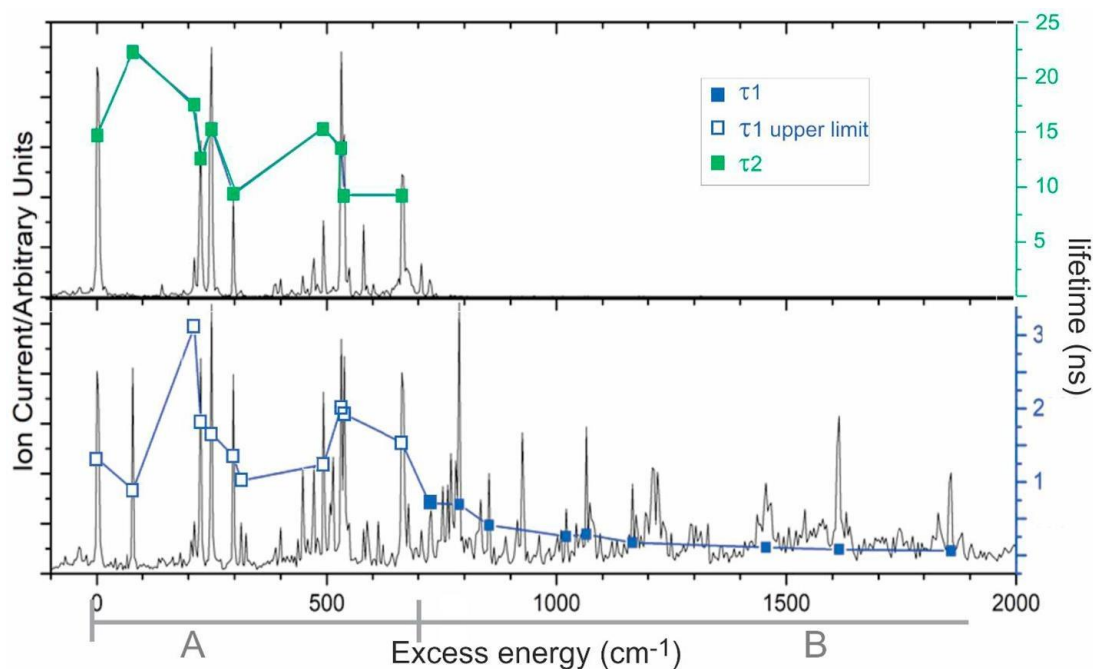


**Figure 3. 2C-R2PI spectra collected using ps excitation followed by ionization with nanosecond pulses (top panel) and picosecond pulses (bottom panel). Squares represent the lifetimes as recorded from pump-probe measurements in the ns range (green) and ps range (blue). Excess energy at approximately 700cm-1 depicts a barrier where the short lived picosecond component is absent [35].**

10

In conjunction with computational methods, a two-barrier excited state reaction path was observed corresponding to competing proton and hydrogen transfer which depends on vibrational modes, as well as opposite character in the ground state trajectories. The contrast in polarity between ground state and excited state intramolecular proton or hydrogen transfer suggests effects of stabilization by different polar solvents or chemical modifications [35]. Although further evidence is needed, hydrogen transfer might be associated with the faster decay channel and that the probability of internal conversion is greater at higher excitation energies. It is also possible that proton transfer and hydrogen transfer processes can interconvert via intramolecular vibrational energy redistribution (IVR), but further evidence is needed. This study further supports that gas phase experiments provides a bottom-up approach can provide a comprehensive framework for studying the dynamical behavior of complex systems. Molecular spectroscopy is a powerful tool to bridge our understanding of ESIPT and its dynamics. To expand this study using this technique, the effects of deuterium substitution will be observed to elucidate the effects of tunneling on the relaxation pathways of the mono-enol tautomer in the $S_1$ state.
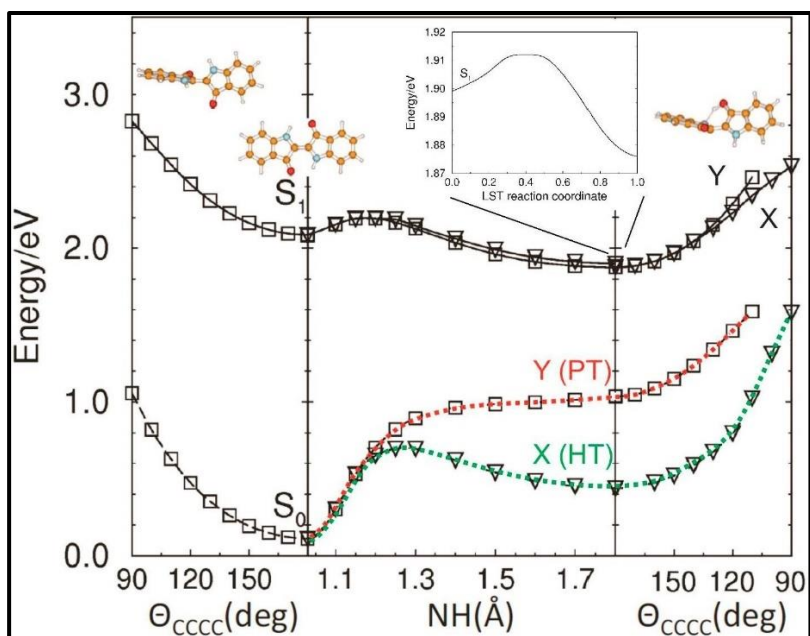
**Figure 4. ESIPT reaction PES of indigo with geometries of ground state in the center, inter-ring twist of diketo tautomer on the left, and mono-enol tautomer on the right. Solid lines denote minimum-energy profiles of the S1 state. Dashed lines denote vertical-energy profiles of the ground state computed at the geometry of the S1 state. X form represents PT tautomer and corresponds to square and red lines. Y form represents HT tautomer and corresponds to triangles and green lines. Inset illustrates the barrier which separates the two tautomeric forms computed along the Linear Synchronous Transit (LST) reaction path connecting the S1-state optimized geometries of the X (left) and Y (right) conformers [35].**

## II. Spectroscopic Technique

### A.  *Method Overview*

The study of biomolecules often involves the use of solvents, which blurs fundamental intrinsic properties of a molecule due to a myriad of intramolecular interactions. Hence, to capture the nature of an isolated molecule, considerable analytical progress has improved conditions of gas phase studies, allowing sensitive and controlled studies of ultrafast photochemistry of biomolecules. Gas phase spectroscopy offers sensitive probing of structural features, such as isomer selectivity. By examining a biomolecule independently of solvents, a bottom-up approach provides a better context of more complex interactions. This section will detail a home-built combined instrumental technique consisting of (a) laser desorption, (b) jet cooling, (c) photoionization, and (d) mass detection via time-of-flight mass spectrometry (LD-JC-REMPI-MS). The experiments were carried out in a well-defined clean ultra-high-vacuum environment provided by two diffusion pumps operating at $2 \times 10^{-5}$ torr by a diffusion pump (Edwards Diffstak 250, 2000 L/s) for the chamber housing and $2 \times 10^{-6}$ torr (Diffstak 100, 280 L/s) for the time-of-flight tube. This technique provides exceptionally well resolved vibronic spectroscopy and fragment-free spectroscopy for molecules of interest by combining multiphoton ionization with mass spectrometry. Each component of these experiments serves a vital role in providing highly resolved spectra of discrete energy states of molecules and the basis will be described in detail in the sections below. The combination of laser spectroscopy and mass spectrometry provides analytical information in two dimensions: wavelength and mass. Two-dimensional spectroscopy allows for identification of molecules not only by their mass but also by their typical optical

molecular spectrum. By separation of the two lasers used for desorption and ionization in space and time, low fragmentation of the parent species is achieved. One of the challenges in analyzing biomolecules is its degradability at high temperatures and low vapor pressure. Using a high energy and fast pulsed laser to desorb the molecules into the gas phase, avoids fragmentation. The desorbed molecules stay in their neutral form and do not undergo any photochemical interactions at this wavelength. The molecules are entrained in a molecular beam, a pulsed supersonic jet expansion of argon that efficiently lowers internal temperatures to several tens of degrees Kelvin or below which provides high resolution REMPI spectra. By studying neutral cooled gas phase species, noncovalent interactions such as hydrogen bonding, base stacking, and charge transfer can be studied through this technique. Downstream, the molecules are carried to the extraction field of a time-of-flight mass spectrometer. The molecule is intersected by multiple photons, where it is resonantly excited and ionized. A first photon, tuned to a resonant vibronic transition, excites the molecule to an excited electronic state. This step utilizes wavelength selectivity, allowing for ionization of the analyte of interest irrespective of the matrix and complexity of the sample and hence, minimizing sample preparation and purification steps. Next, a second photon ionizes the excited molecule, and the ions are detected in the TOF mass spectrometer. By using two different lasers we can independently optimize the excitation and ionization steps for maximum detection efficiency without sacrificing selectivity. We have demonstrated near unity two-step photoionization efficiency, leading to attomole detection efficiency. Thus, this technique requires minimal sample size, making it an ideal analytical method for projects such as archelogy, art preservation, and analysis of extraterrestrial samples. Resonant ionization not only selects for a specific compound; it can

also select for specific isomers. We employ spectral hole burning coupled with REMPI to obtain an IR spectrum of individual isomers. In this approach a tunable IR pulse resonantly modifies a specific population in the molecular beam before excitation, which we detect as a change in the ion signal. The resulting isomer selected IR spectrum allows for structural identification. Our technique is specifically designed to study aromatic molecules. This combined approach is a powerful technique that can achieve structural resolution for isomeric specificity, minimize sample size and processing, and provide background discrimination against a matrix of compounds. This technique has been used for analytical applications and the study of UV photochemistry. Parameters have been extensively optimized. A schematic is shown below.
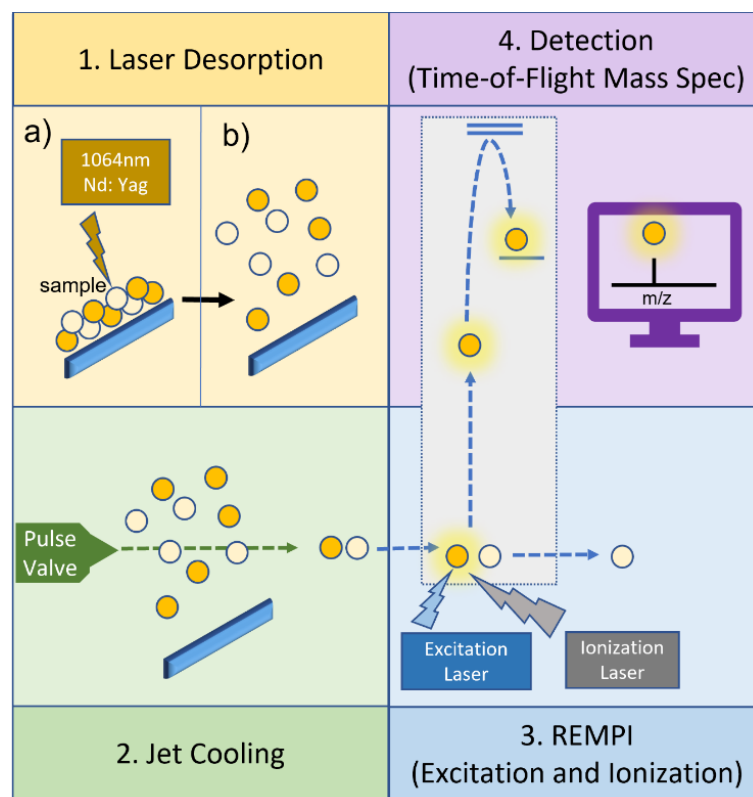


**Figure 5. Schematic of technique. 1) Laser desorption: a) Sample on a translating graphite bar is laser desorbed by a focused Nd:YAG pulse (1064 nm, ~1 mJ/pulse) operating at 10 Hz, b) volatilizing low vapor pressure molecules without fragmentation**

**or degradation. Dark and light yellow represents different conformations of a single molecule. 2) Neutral molecules are entrained in a supersonic expansion from a piezo pulse valve ((8 atm backing pressure, 30 µs pulse width), which entrains the gaseous molecules and lowers the internal temperature to several tens of degrees Kelvin or below. 3) Cold gaseous molecules are selectively ionized by wavelength using REMPI techniques and is then 4) detected by a reflectron time-of-flight mass spectrometer.**

### B. *Laser Desorption*

For these experiments, it is essential to conduct them in gas phase, as the goal of the study is to elucidate the intrinsic photochemical properties of a molecule. Solution phase studies complicates experiments as solvent interactions contributes to spectroscopy. There are many ways to volatilize a solid sample. A simple approach would be a direct heating method using a hot pulsed or continuous oven. This technique is limited to molecules with low volatility which can be heated into gas phase. This presents a problem for molecules that are nonvolatile and thermally labile, as they will decompose upon heating. A way to circumvent this limitation to include nonvolatile molecules is by chemical derivatization of polar groups to produce molecules with higher vapor pressures. The consequence is a large increase in molecular weight, proportional to the number of polar groups. For the nature of our experiments, the approach should consider fragile high molecular weight samples, keeping the molecule intact and in its original chemical form. In addition, the need for a direct, facile detection of the molecule in heterogenous sample with little to minimal sample preparation.

Laser induced desorption of surface bound gases was reported as early as 1967 by Levine and coworkers [36]. In the late 1970s, Posthumus et al. were the first to volatilize polar, nonvolatile organic molecules, producing intact gas phase molecule using laser induced desorption technique. They used a sub microsecond laser pulse to volatize oligosaccharides, which are notorious for their nonvolatility and thermal lability, from a thin

16

layer of sample coated on a metal surface and detected by mass spectrometer. However, during the laser desorption process, cationized species were produced rather than neutral species [37]. Several groups have since studied laser desorption of organic molecules from surfaces [38]. A decade later, Levy et al. were able to observe high resolution gas phase electronic spectra of peptides seeded in a supersonic molecular beam by laser desorption [39]. Continued efforts by Lubman coupled pulsed laser desorption with jet cooling to produce sharp spectral features of nonvolatile thermally labile molecules such as amino acids, probed by resonant two-photon ionization spectroscopy in a time-of-flight mass spectrometer [40] [41]. Continued efforts by Meijer et al. studied the cooling characteristics and detection sensitivity of laser desorption jet-cooling of organic molecules and were able to detect as little as 30 picograms of materials by wavelength and mass. This highlights wavelength-selective as well as mass-selective detection of molecules desorbed from a surface without fragmentation. [42] [43] [44]. The emergence of matrix assisted laser desorption/ionization (MALDI) and electrospray ionization (ESI) as a powerful technique for producing intact ions extended the application of mass spectrometry to large fragile biomolecules including oligonucleotides and proteins [45].

Laser desorption can take place in different ways such electron stimulated desorption (ESD) which is a nonthermal process, and laser induced thermal desorption (LITD) [46]. The latter will be used in the experiments. ESD is based on local electronic excitation at the surface, that can be described by the Menzel-Gomer-Redhead's (MGR) model [47]. First the adsorbate is excited into an antibonding electronic state, then quenching or delocalization of the excitation leads to desorption. LITD is widely used for a variety of applications, such as annealing surfaces [48], to study adsorbates on surfaces [49], and to desorb and ionize large

organic molecules that easily decomposes [50]. The mechanism of LITD is not fully understood but has been described as a thermal model. LITD is a technique where a high-powered pulsed infrared laser is used to induce a rapid heating that gently but rapidly vaporizes the sample from a surface. The adsorbate molecule does not receive energy directly from the laser radiation. Instead, intramolecular vibrational energy transfer flows from the hot surface to the cold adsorbate species, breaking weak van der Waals bond between molecule and surface. The bonds holding the adsorbed species are put into such high vibrational states that they break [51]. This occurrence can be described by the bottleneck effect, which was recognized by Lucchese and Tully who carried out quantitative calculation using stochastic trajectory technique to study desorption of nitric oxide molecule bound to LiF. The bottleneck effect can be described as energy flow from the adsorbate-surface bond to the chemical bonds in the adsorbate [52]. In other words, the physisorption bond serves as a bottleneck for energy transfer from a rapidly heated surface to the internal degrees of freedom of the adsorbed molecule. The frequency mismatch in which the low frequency surface mode coupled to high frequency molecular modes allows for the rapid heating rates, thereby achieving desorption [53]. Neutral species are the major product of the desorption event, which is key for the technique as described in the next section describing spectroscopic detection. LITD depends a great deal upon the temperature or heating rate, which needs to compete against vibrational excitation that is responsible for fragmentation. Reactions will dominate at slow heating rates and desorption at rapid heating rates [54]. LITD allows the surface to be heated at rates up to $10^{11}$ K/s with nanosecond laser pulses, whereas conventional heating and electron bombardment can only achieve heating rates up to 10K/s and $10^3$ K/s, respectively. This rapid heating rate induced by a laser can favor desorption

18

over decomposition and is key to desorption [55]. Deckert and coworkers describes the relationship between surface heating rates and the yields for desorption and reaction as a 1:1 ratio. One limitation to this method is the maximum temperature of the surface before melting of the surface occurs. Hence, selection of substrate will be limited to the material that has a melting point greater than the required peak temperature on the surface. [56]. Parameters that influence desorption yields include but are not limited to laser pulse length and shape, kinetic parameters, and peak temperature reached on the surface [57] [58]. Choice of substrate can influence desorption efficiency, as the material can range from glass, graphite, gold plated copper, stainless steel and more [59].

In these experiments, the desorption laser is focused on the surface of a graphite bar. Graphite absorbs at 1064 nm which does not overlap with the absorption spectrum of the adsorbate. Therefore, we were able to perform laser desorption experiments using the fundamental of a Continuum Minilite YAG laser. The laser is attenuated, and levels of attenuation is optimized based on signal intensity. The beam is focused and directed onto the graphite sample bar, which is placed on a motorized translating sample holder in order to expose fresh sample between successive laser shots. The desorbed neutral molecules are entrained in a supersonic jet expansion as described next.

### C. Supersonic Jet Cooling

Once the molecules are in neutral gas phase, the next step is to cool them. Cooling reduces the number of populated molecular rotational and vibrational modes for highly resolved resolution in spectroscopy. Large molecules at room temperature can occupy millions of states will have a large density of states, resulting in a spectrum with broad diffuse features that is difficult to resolve, interpret, and assign. The broad bands are due to

hot band absorptions, transitions originating from thermally populated vibrational and rotational levels which are dependent on the temperature of the sample. By lowering temperatures, electronic absorption and emission spectra consist of sharp lines rather than broad bands. Hence, producing internally cold molecular species is an essential step in exploiting molecular 'fingerprints' in chemical analysis.

Temperatures much below the freezing point of the sample will be necessary for producing low internal temperatures and thus, traditional methods of freezing will not suffice. Supersonic jet cooling is a cooling technique that produces cold, isolated, gas phase molecules without matrix or collisional perturbations and condensation, providing narrow bandwidth character of a spectrum. It produces translational and rotational temperatures below a few Kelvin. Supersonic molecular beams were introduced theoretically by Kantrowitz and Grey, and experimentally by Kistiakowsky and Slichter in 1951 [60] [61]. In 1975, Levy and coworkers coupled supersonic jet cooling with high resolution spectroscopy, which revolutionized molecular spectroscopy. [62]

The principle of jet cooling is to convert random molecular motion into directed mass flow along the beam axis, in which rapid expansion adiabatically cools the sample to produce a beam internally cold molecules with high forward supersonic velocities. This is established when a relatively high-pressure gas is expanded from a reservoir into a vacuum through a small orifice. [63] The reservoir contains high pressure inert gas of random molecular motion represented by a Maxwellian distribution at the equilibrium reservoir temperature. The molecular mean free path between collisions is much smaller than the orifice diameter, allowing the orifice to act as a supersonic nozzle or jet. [64] Of the many collisions in the vicinity of the jet orifice, only those which have achieved a large velocity

component in the axial direction are able to escape the reservoir. This results in directed mass flow of the gas, a supersonic jet, outside the orifice in which the expansion proceeds faster than the speed of sound in the vacuum. [65] This relationship can be described by the Mach number $M$, which increases as flow velocity, $u$, increases and the speed of sound, $a$, decreases in the expression $M = u/a$. Supersonic expansion is achieved when $M = 1$ near the nozzle and $M > 1$ downstream from the nozzle. This speed produces a shock wave called the Mach disc, which protects region of the beam from interaction with background gases and pressure changes. [66] At the core of the jet, density and collisions are decreased and the system may be in a highly nonequilibrium state. As a result, rotational and vibrational energy distributions are decreased and essentially 'freeze' when collisions are negligible. The gas is then cooled by providing energy to the conversion of directed mass flow from random motion requires energy. The width of the velocity distribution determines cooling efficiency. Large molecules can be rotationally cooled to below 1K while vibrational and translational energy can be cooled to 10 to 20K. width of the velocity distribution. Condensation does not occur because it is a much slower process than rotational and vibrational relaxation. Significant analytical power is unleashed by combining laser desorption and jet cooling. In these experiments, high purity argon gas with a backing pressure of $6 \times 10^3$ torr flows through a conical shaped pulsed nozzle (Amsterdam Cantilever Piezo Valve ACPV2), entraining freshly desorbed gas phase species in a high vacuum chamber with a pressure of $2 \times 10^{-5}$ torr. This low pressure is maintained by large diffusion pump (Edwards Diffstak 250, pumping speed: 2000 L/s). In addition, the pulsed piezo valve operating at 10 Hz repetition rate prevents gas overload on the diffusion pumps. Conditions such as timing between laser desorption and pulsed valve opening, pulse width, and pressure

are optimized as clusters can sometimes be formed in the expansion. The cooled gaseous sample is skimmed by a 3mm skimmer and enters the source where it is then ready for ionization and detection.
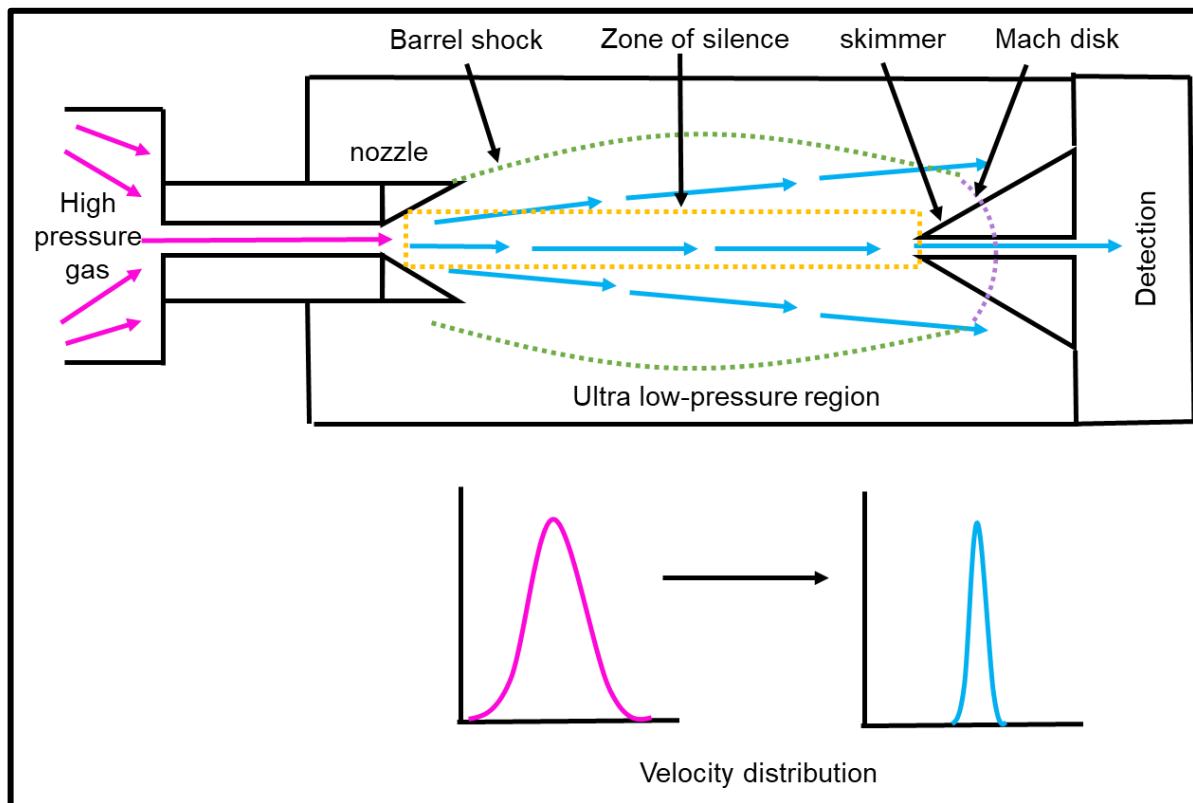


**Figure 6. Schematic diagram of supersonic jet cooling. First, high pressure gas expanded through a pulsed nozzle into a region of ultra-low pressure. Random thermal motion of the gas molecules (pink arrow) is converted into directed kinetic motion (blue arrow). The zone of silence in dotted orange lines is the region of expansion where the Mach number (M) >> 1 and this is the collision free region. The dotted green lines are the outer limits of zone of silence and separate this region from the barrel-shock region containing pressure shock waves. The result is a narrow velocity distribution, providing low translational temperature.**

### D. Photoionization

In selecting a spectroscopic technique for ionization in this application, the method must a) be highly sensitive due to low density of molecules in the molecular beam, b) enable the elucidation of photochemical properties of the molecule of interest and c) result in ionization

22

without fragmentation for detection. Photoionization is the process of ionizing molecules when the molecule absorbs a photon or photons that has energy greater than the ionization potential of the molecule. The energy of the photon E can be represented by the equation

$$E = h\nu \hspace{4cm} Eq\ (5)$$

where h ($2\pi\hbar$) is the Planck constant, $\nu = c/\lambda$ is the photon frequency; $\lambda$ is its wavelength, and c is the speed of light. When a molecule absorbs light, it undergoes a transition from an initial state to a final state with the energy difference E. The transition can be radiative or non-radiative transitions. This work will focus on non-radiative transitions, which occur through intersection of the potential energy surfaces of the electronic states involved in the transition. Energy transfer processes can be monitored on potential energy surfaces, a multidimensional topology that is a function of molecular potential energy and internuclear distance. In the Born–Oppenheimer approximation the nuclear and electronic part of the wavefunction can be separated and approximated, allowing for calculation of the adiabatic potential energy surface of a fixed nuclei at defined positions. The Franck-Codon principle states electronic transitions are much faster than nuclear rearrangement, making electronic transitions instantaneous and therefore, the vibrational state of the upper electronic level that has the greatest overlap with the original state vibrational wavefunction will be occupied as indicated by a vertical arrow. The relative intensity of each transition depends on the absorption strength, often referred to as the oscillator strength, which describes the probability of the transition between the initial and final states. The interaction strength between light and the molecule is dependent on the magnitude of the transition dipole moment of the initial and final states which is dependent on the charge distribution during transition, the overlap between the vibrational states of initial and final electronic states.

23

Most organic molecules have an ionization potential between 7 and 13 eV. In these experiments, a form of photoionization called resonance enhanced multi-photon ionization (REMPI) is used. REMPI is a highly effective and sensitive spectroscopic method used to study the quantum states of free molecules. In REMPI, a molecule absorbs multiple photons that excite the molecule through allowed vibronic transitions (M → M*) and is then ionized from real excited states (M* → M+) (67). Vibronic transitions in turn induce rotational transitions, resulting in multiple absorption lines. Thus, a requirement of this technique is that the analyte must have a chromophore, a part of the molecule that can absorb light. It is important to note that REMPI is a form of action spectroscopy, in that it does not directly measure the photoabsorbance of the molecule but rather the effect of light on the molecule. The types of REMPI techniques discussed in this section are illustrated in Figure 7.
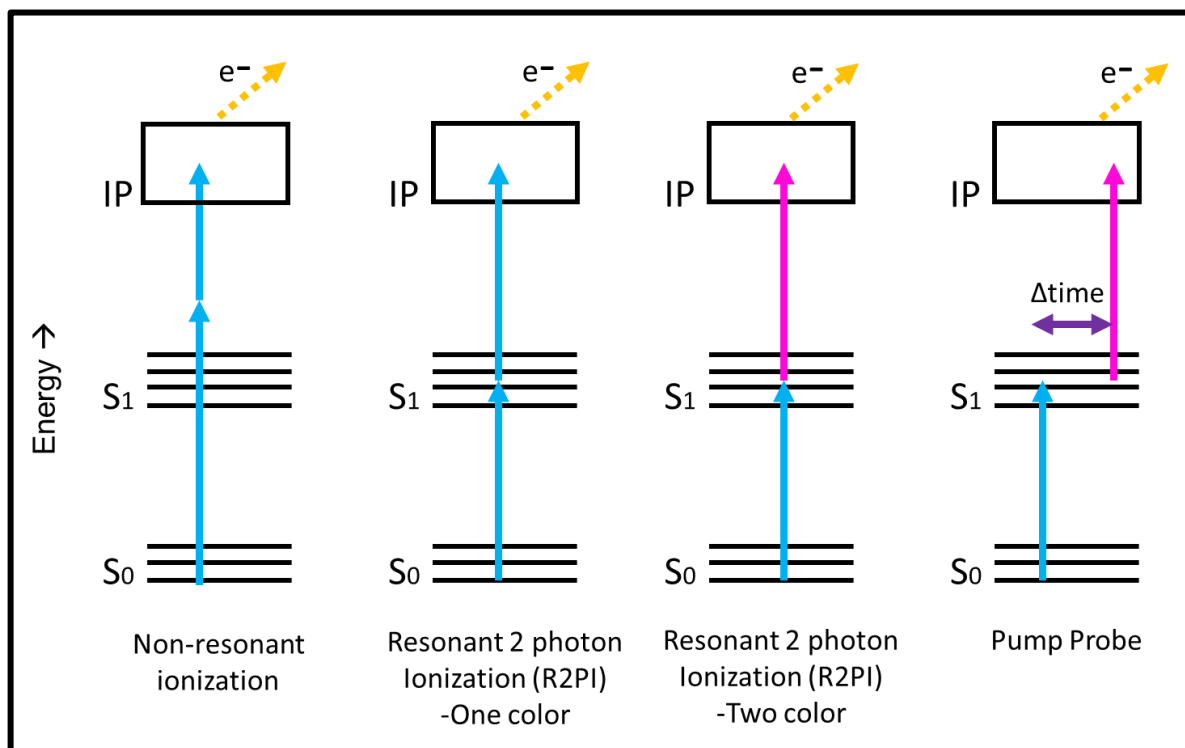


**Figure 7. Jablonski diagram of non-resonant ionization and REMPI techniques including one color R2PI, two color R2PI, and pump probe that allows for transition $S_0 \rightarrow S_1$ and ionization at the ionization potential (IP).**

24

Resonance ionization spectroscopy was first performed in a gas cell by Johnson in the mid-1970s [68] [69]. Rapid advances in this technique allowed for the investigation of previously inaccessible electronic transitions and vibronic states of diatomic and polyatomic molecules with the advent of wavelength tunable lasers [70] [71]. REMPI was combined with the supersonic beam in the late 1970s and in the 1980s was investigated with laser desorbed neutral molecules, both of which provided for the isomer and isotopic isomers selectivity. In the mid-1980s, the wavelength tunable picosecond laser unleashed the power of probing fast nonradiative processes. Picosecond chemical timescale corresponds to intramolecular energy redistribution which is faster at higher internal energies and time between collisions in the gas phase. At the intramolecular timescale, rotational motion is slower for large molecules with large moments of inertia in the picosecond range. Nanosecond timescales typically corresponds to radiative decay from electronically excited states. This suggests the laser pulse requirements should be short enough to localize the motion within the range of distances that is to be probed.

REMPI is a powerful spectroscopic technique that allows sensitivity down to the ppb and ppt level, providing comprehensive knowledge for analytical applications. Resonant ionization has many spectroscopic advantages as opposed to non-resonant ionization. In non-resonant ionization the molecule is excited to an extremely short-lived virtual state by a photon and ionized by another photon. These virtual states are difficult to access and has less molecular specificity. In resonant ionization, the intermediate state can be selected so that a broad range of original rovibronic levels in the ground state can be reduced a limited number of intermediate states. Since the molecular beam contains a low molecular density, high ionization efficiency is critical. Ionization efficiency depends on the energy match

between photon and intermediate states and photon density. REMPI is enhanced with molecular cooling and thus reducing congestion. Ionization can involve molecular absorption of one photon, which is a form of non-resonant ionization methods or two photons, which is resonant ionization technique. With resonant two-photon ionization or R2PI, one photon electronically excites the molecule of interest from the ground state and a second photon to ionize that excited molecule. Although the requirement is that the first photon is resonant, the second photon does not need to be resonant since the photoelectron can remove excess energy during the ionization. One advantage of this technique is that the resonant state is often in a more favorable Franck-Condon regime to ionization than the ground state. The ionization potential is reduced, minimizing available excess energy to the molecule and fragmentation making this technique a soft ionization process. On the other hand, one photon ionization, will require significant energy to cross the target ionization potential since it is one step ionization process and may result in fragmentation of the molecule. The energy of the photons is typically in the vacuum ultraviolet region of < 200 nm. This poses a problem for studying conjugated systems that serve as chromophore. However, an advantage of one photon ionization is that it does not require knowledge of the molecule's potential energy surface since it does not have to be tuned to an energy level, which may be useful in simplifying analytical studies.

R2PI can be one color or two color. One color R2PI utilizes one wavelength for excitation and ionization, whereas two colors R2PI uses different wavelengths for excitation and ionization. Since one color R2PI utilizes one wavelength for both excitation and ionization, they can come from the same laser and therefore do not need to be spatially and temporally overlapped, whereas in two colors R2PI this step is necessary. A problem with

using one color R2PI may arise when second photon is not sufficient to reach ionization potential which varies by analyte. Another issue with one color R2PI is that because Since ionization efficiency is dependent on the photon energy available in ionization, excitation may become saturated because ionization has a smaller cross section than excitation [72] [73]. In two color R2PI, each step can be fine-tuned to avoid spectral broadening due to saturation. Broadening can be due to several effects such as doppler broadening. Doppler broadening is contributed to a spread of frequencies absorbed by molecules moving in different directions, as absorption is different for a stationary molecule and a moving molecule.

The studies mentioned here utilize two colors R2PI combining laser desorption and jet cooling to achieve a resolved spectrum containing many bands that are attributed to transitions from the ground state to excited electronic states and to vibrational states within an excited electronic state. The pulse arranges the molecule in a defined excited electronic state but in a range of final vibrational states. The collision free region of the molecular beam at the source is intersected with lasers to probe by wavelength using two color R2PI, then detected by mass.

In these experiments, the excitation laser is scanned in the region of interest while monitoring the ion signal produced by a fixed ionization laser. Two ultraviolet (UV) photons are sufficient to cross the ionization potential for most organic molecules and therefore, both photons are in the UV range. The highly resolved mass spectrum provides information on the electronic energy level of a molecule. When analyzing the spectrum, the transition from the lowest vibrational state in the ground state to the lowest vibrational state in the first electronic state is called the 'origin'. This is the $S_1 \leftarrow S_0$ transition, or the singlet ground

27

state to the singlet first excited state which is the lowest energy transition. Vibronic transitions within the excited state are well resolved in the spectrum due to the coupling of laser desorption and jet cooling. These transitions provide high specificity, unique characteristics of individual isomers that can be used to gain extensive knowledge of their electronic properties. R2PI can be used as a double resonance technique called UV-UV and IR-UV double resonance spectroscopy, which provide structural information and can be used to obtain signatures for distinguishing between isomers, tautomers, and conformers. When combined with pump probe experiments, the lifetimes of individual isomers can be determined. These techniques are not utilized in these experiments and will not be further discussed as they are described elsewhere, although they contribute significantly to the research of the de Vries group [74; 75; 76].

Ultrafast laser pulses allow probing of electronic transitions on their natural timescale, which are much faster than atomic motion on molecular scales. When a molecule is excited, an initially localized nuclear wave packet can be prepared via coherent excitation of several vibrational eigenstates. The time evolution of the wave packet on the global potential energy surface (PES) is governed by the system's molecular Hamiltonian and reflects the underlying dynamics, either reactive or nonreactive. Zewail's group was the first to observe the coherent evolution of matter wave packets as a single-molecule trajectory with a femtosecond laser, earning the Nobel Prize in 1999 [77]. Typically, electronic state lifetimes and molecular rotations are in the nanosecond timescale and Nd: YAG/excimer lasers could be used. A femtosecond laser pulse such as Ti: Sapphire laser would be used to probe molecular vibrations, and an attosecond laser such as can probe valence band electrons. To measure the excited state lifetimes, the time between the two photons is varied. This method captures the

evolution of the populated $S_1$ ($\pi\pi^*$) state by a time-delayed probe. The excitation laser (pump) is fixed on a wavelength of resonant transition, while the ionization laser (probe) is gradually delayed in time. This results in a ion signal decrease, or a decay trace. Once the decay trace is obtained from pump probe experiments, it must be fitted using pre-exponential factors to derive a lifetime. The time varied in these experiments are in the picosecond and nanosecond time regime. A limitation on lifetime measurement is the dependence on the laser pulse width. Therefore, nanosecond laser system may be blind to nanosecond lifetimes. A key difference between picosecond and nanosecond experiment is the trade-off between time resolution and frequency bandwidth which are inversely related [78].

In resonant excitation, the strength of the optical transition is related to the absorption cross section, which is approximately $10^{-9}$ cm$^2$ in the visible transition, which correlates to a lifetime in the order of 10 ns. Therefore, the probability of achieving a transition requires a photon flux of approximately $10^{17}$ photons cm$^{-2}$ sec$^{-1}$ [79]. This is obtainable for the lasers used in this experiments which includes a picosecond laser system, EKSPLA PL2441, a Nd:YAG laser operating at 10 Hz. The laser fundamental wavelength (1064nm) can be frequency doubled (532nm), tripled(355nm) and quadrupled(266nm) by inserting into corresponding temperature stabilized nonlinear crystals in the beam path. To produce tunable wavelengths for excitation, this laser pumps 8mJ of vertically polarized 355nm into EKSPLA PG401-SH, an optical parametric generator (OPG). The OPG can produce wavelengths ranging from 210nm to 2300nm with a spectral width of 6cm$^{-1}$. To produce the second photon for ionization in two color R2PI experiments, excess frequency doubled harmonic is used to generate 266nm in the pump laser. Exterior of the pump laser, it is

29

frequency mixed with excess fundamental by a fifth harmonic BBO crystal to produce 213nm, which is used as the probe beam. It is important to note that for picosecond experiments, both photons for excitation and ionization are being generated from the same pump laser but have different paths and optics. For picosecond pump probe experiments, the delay ionization is achieved by mechanically increasing the beam path during the experiment. This is performed by a Thorlabs LTS300 stepper-motor driven long travel stages with ranges of 150mm and 300mm with a stepping accuracy of less than 0.5 um. In these pump probe experiments, the motor steps 1mm, in which 1mm correlates to 6.67 picoseconds with 1800 picoseconds maximum, which is limited by the length of the delay stage. A UV coated, broadband retroreflector is mounted on the delay stage, doubling the path length of the ionization beam. After the delay stage, the ionization laser is collimated with the excitation laser. Along the path of the 213nm ionization path are 213nm dichroic, whereas the excitation laser path involves broadband dichroic. In nanosecond pump probe experiments, the delay of the ionization laser is achieved by electronically using a digital delay generator, (Stanford Research Systems, DG645) which provides a range up to 5 ns resolution.
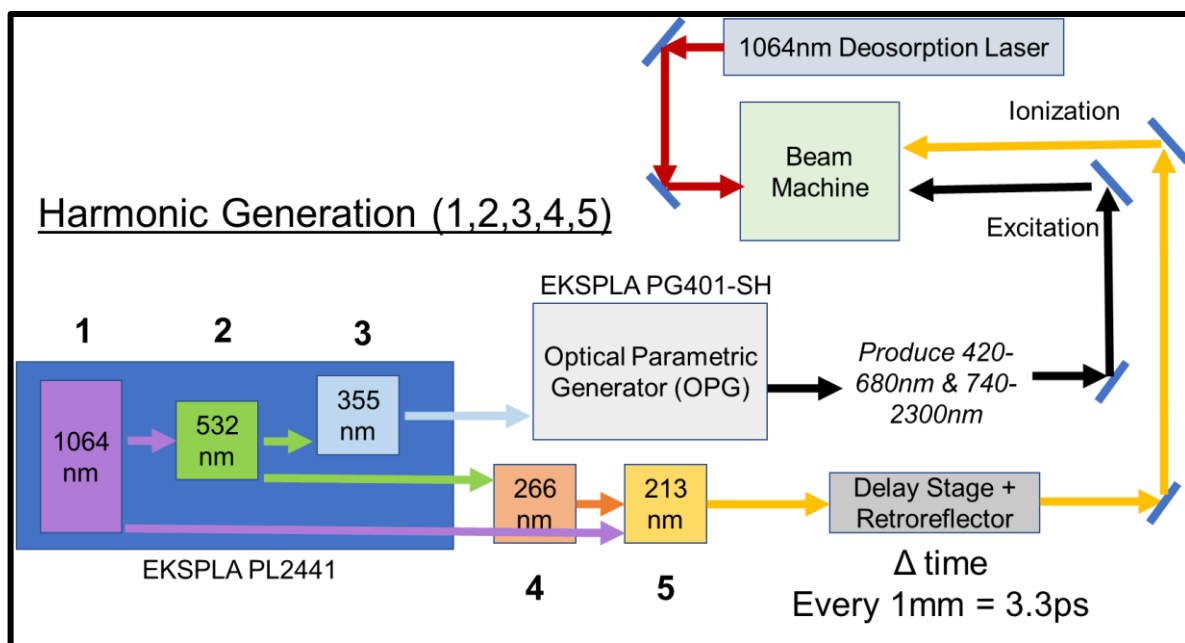
**Figure 8. Schematic of laser set-up for the beam machine. EKSPLA PL2441 produces 1st, 2nd, and 3rd harmonic, to externally produce 4th and 5th harmonic and pump EKSPLA PG401-SH (OPG), which produces a tunable wavelength between 420nm-2300nm. This excitation laser is spatially and temporally overlapped with the ionization laser, produced by the 5th harmonic, and delayed in pump probe experiments with a delay stage. 1064nm is produced from Nd:YAG for desorption.**

### E. Time of Flight Mass Spectrometry

Mass spectrometers are one of the most universal and important tools in scientific research. The first functional mass spectrometer was built in 1919 by Aston who received a Nobel Prize for this work (80). Mass spectrometry allows for highly accurate mass assignment but provides limited information on its own. Its broad range of applications was recognized as tremendous improvements were made on analyzers, ion sources, and ion detection techniques. Several methods of the mass spectrometers were developed, such as time-of-flight mass spectrometer (TOF-MS), which measures an ion's time of flight to determine its mass to charge ratio. [81; 82; 83] Many scientific achievements have been made possible by applications the TOF-MS, especially through the improvements made by Wiley-

McLaren [84]. In 1988, Tanaka was able to ionize proteins as large as approximately 34,000 Da using laser desorption ionization time-of-flight mass spectrometry and received a Nobel Prize for this work [85]. TOF-MS has several operational modes to such as magnetic sector, quadrupole, tandem TOF-MS, matrix assisted laser desorption ionization (MALDI) TOF-MS, and the reflectron TOF-MS (re-TOF-MS) [86]. The re-TOF-MS technique will be explained in detail as it is used in these experiments. Generally, in re-TOF-MS ions are formed in a region called the source, where they are accelerated out from towards a continuously applied electric field. All ions slightly different kinetic energies due to their spatial distribution, which is compensated by a reflectron. The ions travel through a free flight path, and the velocity is determined by the ratio of the charge, $q$, to their mass, $m$. When re-TOF-MS is combined with REMPI techniques, the ion signal reflects the absorption cross section of the resonant intermediate state. Combining detection by mass and wavelength provides unambiguous identification in this approach. This section will detail the four main parts of the re-TOF-MS, comprising of a) the ion source, b) the flight tube, c) the reflectron, and d) the detector [87].

The ion source is the area where the cold desorbed molecules intersect with the ionization laser, gets positively charged, and repelled out of the source and into the TOF tube. The source region is cooled by liquid nitrogen in a baffle to reduce noise. The ion source consists of three planar and one perpendicular electrodes: repeller plate, extraction grid, acceleration grid, and steering plates, respectively. In this setup, the ion source is a dual stage because there are two regions that accelerates the ion: the extraction region and the acceleration region. These separate regions serve to configure the position in time with which the ions are formed to achieve the same kinetic energy. The extraction region is

nestled between the repeller plate and the extraction grid, and the acceleration region is between the extraction grid and the acceleration grid. The positively charged ion gets repelled away from the positive electrode, the repeller, and passes through the extraction grid. It enters the acceleration region where the field is stronger and is accelerated with the correct velocity for entry into the flight tube. Ions in motion during extraction can drift off the path to the TOF tube, which can be avoided by steering plates. These perpendicular plates include a positive and negative charged plate, which keeps the ions on path. Since a pulsed laser is used, the ions are pulsed in packets into the TOF tube.

The TOF tube is pumped down to $2 \times 10^{-6}$ torr with a small diffusion pump (Edwards Diffstak 100, pumping speed: 535 L/s). This vacuum enclosure does not have an electric field, making it a 'field free drift region' where there are no external interactions with the ion packets. All ions entering the TOF tube have the same kinetic energy $E_k$ regardless of mass. The relationship is given by:

$$E_k = \frac{mv^2}{2} = zeE \qquad \text{Eq (6)}$$

where '$m$' is mass, '$v$' is velocity, '$z$' is number of charges on an ion, '$e$' is charge on an electron, and '$E$' is electric field. Since velocity is a factor of distance and time, the equation and be rearranged to determine the 'time of flight' $t$ of the ion given as:

$$t = \sqrt{\frac{m}{z}} \frac{d}{\sqrt{2eE}} \qquad \text{Eq (7)}$$

'$d$' is the fixed distance of the flight tube measuring 150cm. '$e$', and '$E$' are constant throughout the experiments and therefore, these values can be negligible. Therefore, the time of flight is directly proportional to the square root of mass over charge. Given that the time of flight is dependent on mass, heavier ion packets will fly slower than lighter ones if both ions have the same charge. This results in separation of ion packets by mass, in which the

lighter ion packets will reach the detector before the heavier ones. The pulsing of ionization provides a time zero and is essential for this technique to be effective.

An issue encountered is that ions will have slightly different initial velocities due to their spatial distribution in the source where they are ionized. For instance, the ion created closest to the acceleration grid will eject faster than the ion further from the acceleration grid. In addition to their spatial distributions, there are time variations from which the ions are ejected from the source depending on their position. The ions within an ion packet closer to the extraction grid will be ejected first whereas the ions further from the extraction grid will be ejected later. The velocity distribution results in an increased ion packet width and hindered mass resolution. The slower ions will eventually get caught up with the faster ions since they are ejected first, converging at a point called the 'primary focal point'. It seems sensible to place the detector at this point to reduce the ion packet width and improve mass resolution. Consider the mass resolution in full width half maximum (FWHM) expressed as:

$$\text{Resolution} = \frac{m}{\Delta m} = \frac{t}{\Delta t} \qquad\qquad \text{Eq (8)}$$

Stationing the detector at the primary focal point consequently reduces the path length and ultimately, time ions are spent in flight. Since the time ions are spent in flight is proportional to resolution, this contradicts the solution. A practical solution is to create another focal point without compensating flight time using a reflectron. A reflectron acts as an electrostatic ion mirror that 'reflects' the ions back towards the detector, correcting for initial velocity differences [88]. First, the ions would pass the primary focal point, reflect off a reflectron by a linear electric field, then converge at a secondary focal point where the detector is stationed. The reflectron accomplishes a secondary focal point when faster ions penetrate deeper into the relatively weak electric field of the reflectron whereas slower ions

do not penetrate as deep. As a result, faster ions travel a longer path whereas slower ions travel a shorter path, creating a secondary focal point where both ions converge. In addition, the reflectron increases the signal to noise ratio and since it increases the overall flight time, resolution is further improved.

Finally, the ions collide into a dual microchannel plate (MCP) detector [89]. The MCP is 2mm thick with an array of tiny tubes, or microchannels, that range from 10-100 μm in diameter. When an electric field is applied to the plates, the microchannel become small electron multipliers. When an ion collides into the MCP, an electron is ejected from the plate surface, resulting in a cascading effect of more electrons ejecting, resulting in large gains. The electrons are measured by a clean plate that acts as an anode and measures the electrical current. A baseline is monitored to compensate for any fluctuations observed during the experiment. Most mass spectra are fragment-free and display a prominent molecular ion peak. This ion signal is a function of flight time, which are in the microsecond range and can be used to determine the mass to charge ratio of the molecule. Theoretically, TOF-MS has an unlimited mass range. The ion signal is amplified by an order of magnitude by means of a pre-amplifier and displayed on an oscilloscope (LeCroy 9350A) or digitizer. LabVIEW software is used to store oscilloscope data. In R2PI experiments, LabVIEW is programmed to collect mass signal as a function of a scanning excitation wavelength. In pump probe experiments, LabVIEW is programmed to collect mass signal as a function of time. As mentioned earlier, the pulsing of lasers is a criterion for the TOF technique. Thus, timing between laser desorption, jet cooling, excitation laser, and ionization laser must be synchronized in order to produce a mass signal. A delay generator (Stanford Research

Systems Inc., DG-645) facilitates the timing between all the events to run experiments at

10Hz repetition rate.
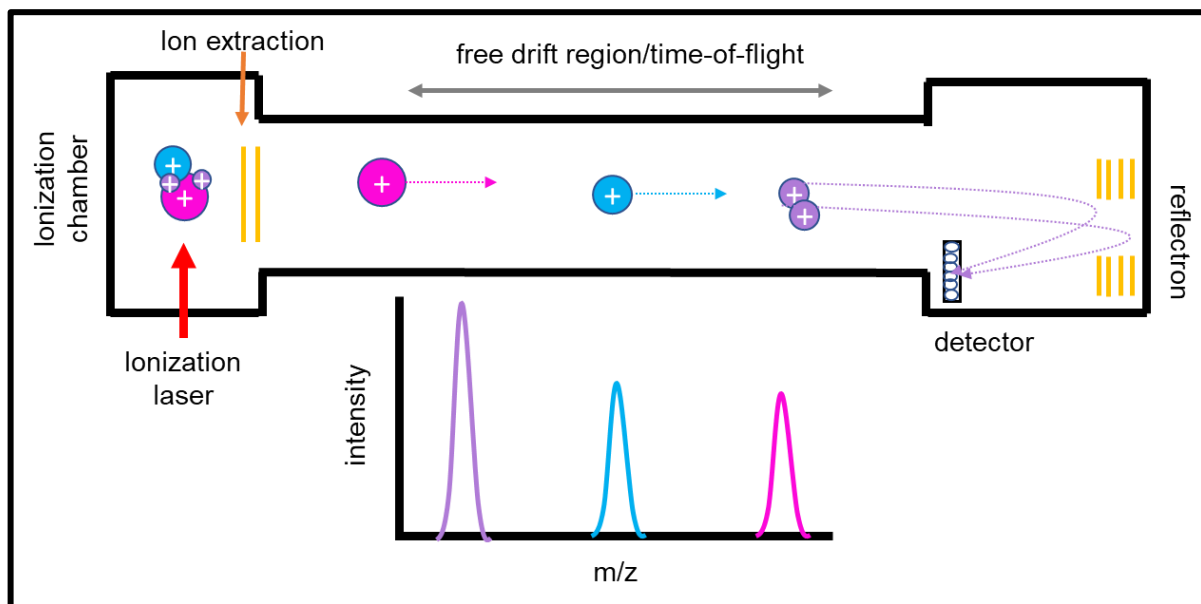


**Figure 9. Reflectron time-of-flight mass spectrometer. The sample is ionized at the ionization chamber by lasers and extracted into the free drift region where it is separated by mass and charge. The molecule with the lightest mass in pink arrives at the detector, followed by the molecule in blue and the largest molecule in pink arrives last. A reflectron placed before the detector is used to correct for kinetic energy differences and extend the path length as seen in the two paths taken by both molecules in purple.**

# III. Isotope Effects on the Excited State Intramolecular Proton Transfer of Indigo

## A. Deuteration of Indigo Dye

Deuteration of indigo dye was prepared in collaboration with Joseph R. A. Kincaid. Indigo, NaOH, and sodium dithionite were added to a vial and purged with argon. Degassed $D_2O$ was added, and the mixture was stirred and heated to 80 °C with until a transparent yellow solution was obtained. The reaction was allowed to cool to room temperature and $O_2$ was bubbled through the solution. The product was a dark blue precipitate that was via centrifugation and washed several times with $D_2O$. Product was then dried on vacuum overnight.
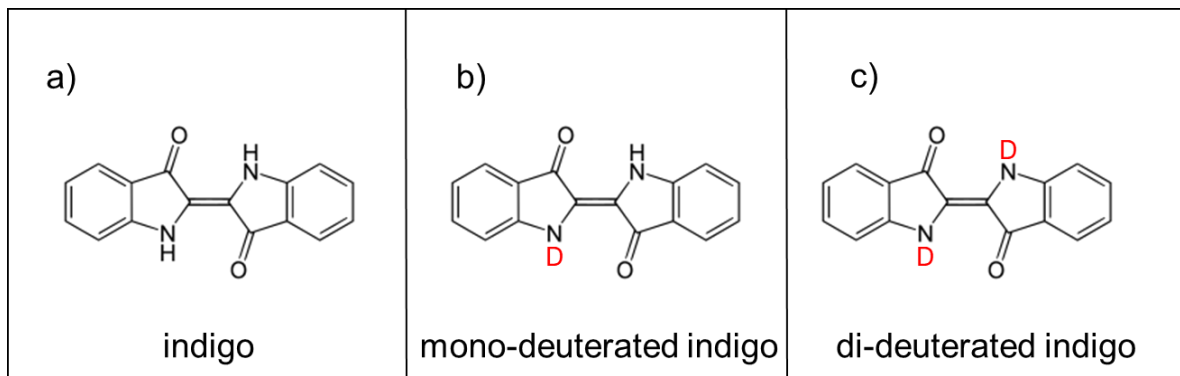


**Figure 10. Three forms of indigo studied in the molecular beam: a) indigo, b) mono-deuterated indigo and d) di-deuterated indigo**

## B. Resonance Two-Photon Ionization Spectra of Deuterated Indigo

The two-color resonance two photon ionization (2C-R2PI) spectra of non-deuterated indigo was previously collected by Haggmark et al. in 2018 [35]. Here, 2C-R2PI spectra is collected for non-deuterated, mono-deuterated, and di-deuterated indigo. These three species were confirmed by the mass spectra displaying three resolved peaks. Each signal was gated

to avoid saturation of the detector and most importantly, to simultaneous monitor the excited state evolution of three systems. The instrument and experimental setup have been described in the previous section. re-TOF-MS voltages and events timing were optimized, resulting in a 20 nanosecond FWHM mass peak of indigo on the oscilloscope. EKSPLA PG-401 optical parametric generator (OPG) produced tunable excitation from 500nm to 560nm (~500uJ output) in 0.1nm increments and ionization wavelength of 213nm (180uJ output) simultaneously generated by the picosecond pump system at 54% amplification to produce the R2PI spectrum of non-deuterated, mono-deuterated, and di-deuterated indigo. In each scan, 30 laser shots were acquired and averaged to produce each data point to minimize the effect of background noise and shot-to-shot laser instability. 3 scans were collected and averaged in the 2C-R2PI spectra in Figure 11.



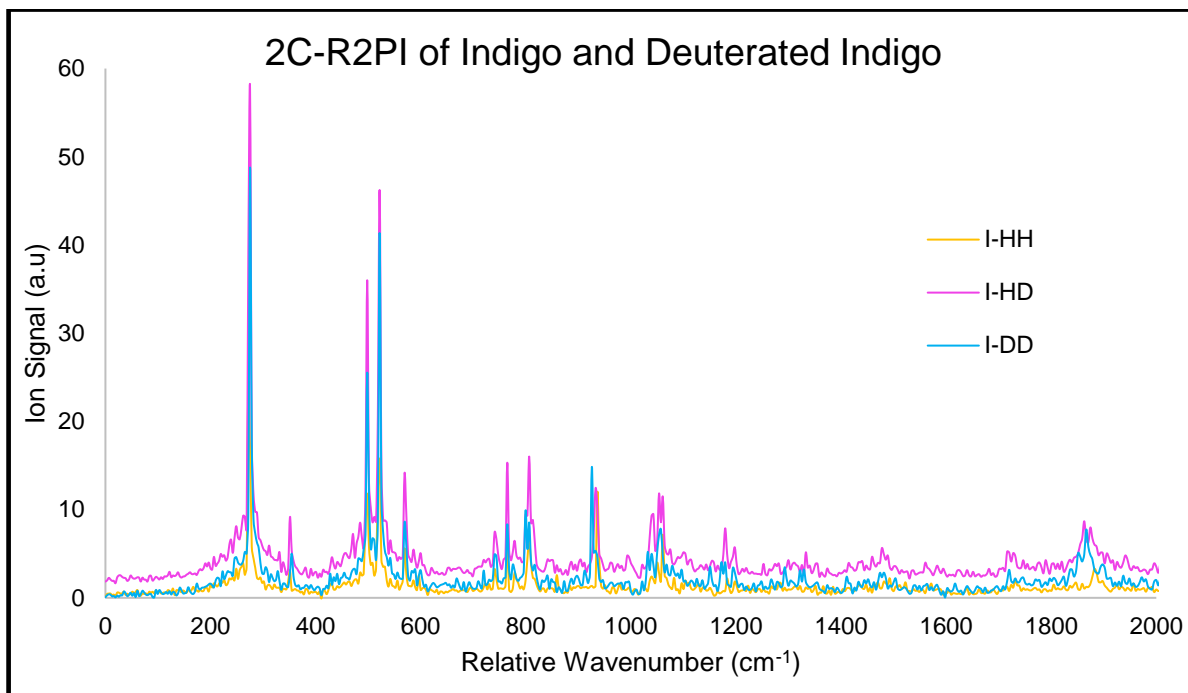**Figure 11. Two-color resonant two-photon picosecond ionization spectrum of jet-cooled non-deuterated indigo in the yellow trace (I-HH), mono-deuterated indigo in the pink trace (I-HD), and di-deuterated indigo in the blue trace (I-DD)**

## C. *Pump Probe Measurements*

Pump probe experiments were performed by delaying the ionization pulse, which is mechanically performed by a delay stage (Thorlabs LTS300) that gradually increases the path length, correlating to delayed ionization. By fixing the excitation wavelength at 549.2nm, its lifetime can be monitored by a decay in ion signal. The setup has been thoroughly described in the methods section. Pump–probe data are collected at $351.2\text{cm}^{-1}$ (549.2nm) and probed with 213nm wavelength. In each scan, the motor steps 1mm correlating to approximately 6.67 picoseconds up to approximately 1800 ps. 10 scans were collected and averaged, each consisting of 30 laser shots that were averaged to produce each data point to minimize the effect of background noise and shot-to-shot laser instability. Decay curves were fitted with a Gaussian fitting model using the following mono-exponential decay function:

$$f(t) = f_0\, e^{-t/t} \tag{9}$$

Lifetimes were derived from kinetic equations and solving ordinary differential equations, involving the instrument response function (IRF), a Gaussian function centered around $t_0$. 811ps was extracted for non-deuterated indigo and 1994ps for mono-deuterated indigo. Mathematical fitting was only performed by Mathematica 10 package on decay traces, although these measurements are in continued works. Note that fitting may significantly vary depending on pre-exponential factors, which predicts the decay and would vary between users.

**Figure 12. Monoexponential fitting method at 549.2nm or 351.2cm⁻¹ for non-deuterated indigo yields an excited state lifetime of 811ps. The IRF is plotted in green.**
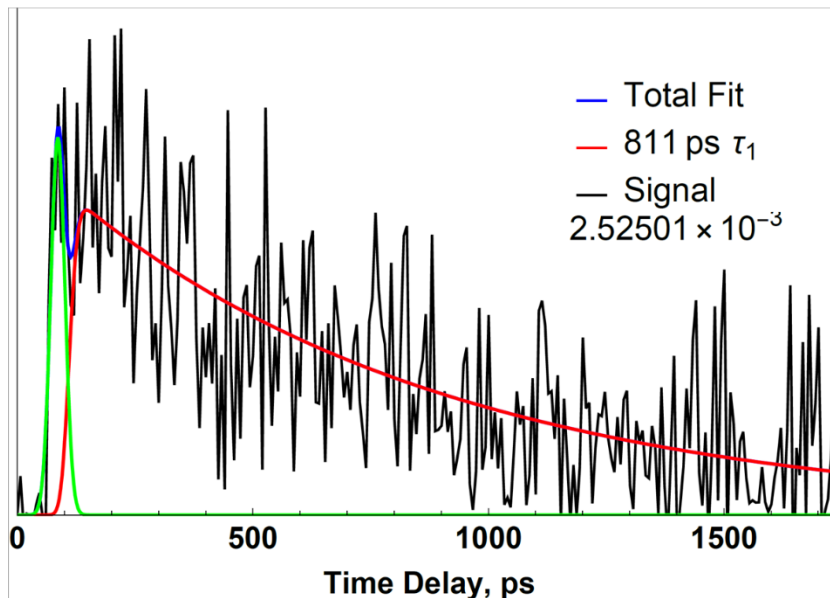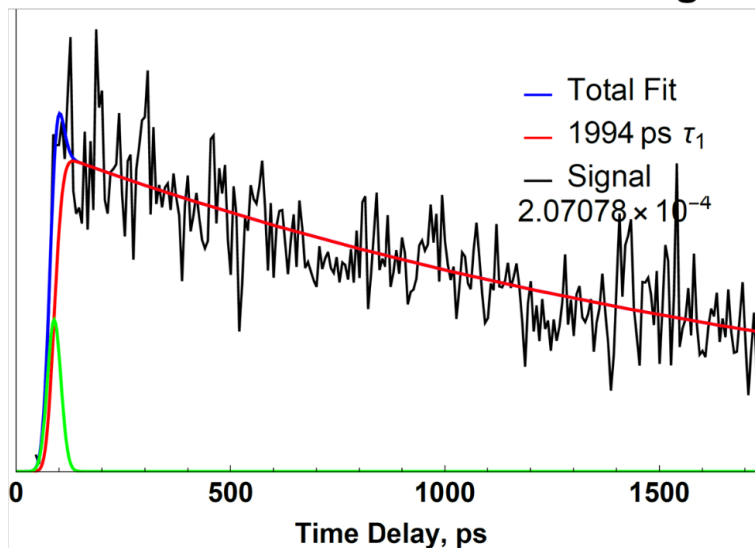


**Figure 13. Monoexponential fitting method at 549.2nm or 351.2cm⁻¹ for mono-deuterated indigo yields an excited state lifetime of 1994ps. The IRF is plotted in green.**

## IV. Discussion and Outlook

This work represents an incomplete collection of data in the following areas: nanosecond pump probe, and picosecond pump probe for all major vibronic bands. Only picosecond pump probe for one vibronic band was performed and fitted monoexponentially which lacks characteristics of a dual relaxation channel. Additionally, only three R2PI spectra were collected for an average whereas typically, more scans would provide more accurate details. This work is being continued along with computational work through international collaboration. The following conclusions can be made based on partial data of this project and will be discussed: 1) in the picosecond 2C-R2PI spectrum of indigo, a red shift and peak splitting is induced upon deuterium substitution on and above the barrier, as well as no shift or blue shift below the barrier, where the barrier corresponds to the separation of the proton transfer and hydrogen transfer forms of the keto-enol tautomer in the $S_1$ state. 2) In pump probe measurements, deuterium substitution induces a longer excited state lifetime with a $k_h/k_d$ ratio of 2.5.

Table 1 provides major vibronic peaks and their shifts due to deuterium substitution effects relative to non-deuterated indigo. The 2C-R2PI spectrum of non-deuterated indigo matches with the 2C-R2PI picosecond spectrum collected from Haggmark et al. using the same technique [35]. The 2C-R2PI spectra of deuterated and non-deuterated indigo have the following differences: a blue shift below the barrier, no shift approaching the barrier, and a red shift at and above the barrier, as well as splitting of peaks above the barrier. In previous fs solvent phase studies of indigo derivatives, the shift induced by deuteration corresponded to coupling of C=O mode with low frequency modes which involves scissoring modes due to bond angle changes associated with deuteron transfer, whereas this feature was not found

in the non-deuterated system [31]. Additionally, this scissoring mode in deuterated system is a slower process than proton transfer in non-deuterated systems. Vibrational-mode-specific tunneling splitting were also observed by Mengesha et al. in isotope effects of proton tunneling in jet cooled porphycenes which exhibits double hydrogen transfer. It was concluded that isotope substitution affects hydrogen transfer even when the weak structural modifications are far from the reaction center, highlighting the strongly multidimensional nature of the tunneling process [90]. This process is entirely dependent on the symmetry of the molecule and may explain why splitting is observed at higher excitation energies in mono-deuterated substitutions in our results.

The rates determined in this experiment reflects the transition state of the recovery process and not the ESIPT directly, as ESIPT occurs in the femtosecond timescale and the lifetimes measured here are in the picosecond timescale. Pump probe experiments allows monitoring lifetimes as a function of excitation energy to understand the excited state dynamics involved in deactivation. Using equation 4 ($k = 1/t$), we can derive the rate of non-deuterated indigo and mono-deuterated indigo from their lifetimes of 811ps and 1994ps respectively, resulting in $1.2 \times 10^9 \, \text{s}^{-1}$ and $5.0 \times 10^8 \, \text{s}^{-1}$. The ratio of $k_h/k_d$ is 2.5, indicating a strong isotope effect. In a femtosecond solution phase study, a rate slow down upon deuteration were observed in fs studies of indigo derivatives, with a $k_h/k_d$ ratio of 1.5 whereas our pump probe studies result in a $k_h/k_d$ ratio of 2.5 [32]. However, it has been found that ESIPT is sensitive to solvent and intermolecular interaction and may attribute to stronger isotope effects observed in gas phase results [34]. The strong isotope effect found in this study indicates that the tunnel effect takes place in the ESIPT of the non-deuterated system.

**Table 1. Vibronic peaks and their shifts in response to the deuterium substation effect, where below, on, and above the barrier corresponds to the separation between proton transfer and hydrogen transfer mono=enol tautomer product in the S1 state.**

| | Wavelength (nm) | Wavenumber (cm⁻¹) | Relative wavenumber (cm⁻¹) | Mono deuterated | Di Deuterated |
|---|---|---|---|---|---|
| Below the barrier | 551.6 | 1812.9 | 271.9 | Blue shift | Blue shift |
| | 549.2 | 1820.8 | 351.2 | No shift | Blue shift |
| | 544.8 | 1835.5 | 498.2 | No shift | No shift |
| | 544.1 | 1837.9 | 521.8 | No shift | No shift |
| On the barrier | 532.1 | 1879.4 | 936.3 | Red shift | Red shift |
| Above the barrier | 528.7 | 1891.4 | 1057.2 | Splitting | Red shit |
| | 524.8 | 1905.5 | 1197.7 | Splitting | Red shift |
| | 521.2 | 1918.7 | 1329.3 | Splitting | Red shift * |

# References

1.  A. Douhal, F. L. (1996). Proton-transfer reaction dynamics. *Chem. Phys., 207*, 477.

2.  A. Douhal, F. L.-R.-G. (1994). Excited-State Proton (or Hydrogen Atom) Transfer in Jet-Cooled 2-(2'-Hydroxyphenyl)-5-phenyloxazole. *J. Phys. Chem., 98*, 12198.

3.  A. Douhal, S. K. (1995). Femtosecond molecular dynamics of tautomerization in model base pairs. *Nature, 260*, 378.

4.  A. E. Cameron, D. F. (1948). An Ion ``Velocitron. *Review of Scientific Instruments , 19*, 605.

5.  A. G., C. (1985). Transient annealing of semiconductors by laser, electron beam and radiant heating techniques. *Rep. Prog. Phys., 48*, 1155-1233.

6.  A. J. G. Strandjord, S. H. (1983). Excited-State Dynamics of 3-Hydroxyflavone. *J. Phys. Chem., 87*, 1125.

7.  A. Kantrowitz, J. G. (1951). A High Intensity Source for the Molecular Beam. Part I. Theoretical. *Review of Scientific Instruments, 22*(5), 328.

8.  A. N. Bader, F. A. (2002). Proton Transfer in 3-Hydroxyflavone Studied by High-Resolution 10 K Laser-Excited Shpol'skii Spectroscopy. *J. Phys. Chem. A, 106*, 2844–2849.

9.  A.A. Deckert, S. G. (1987). Heating rates required for laser induced thermal desorption studies of surface reaction kinetics. *Surface Science Letters, 182*(1-2), L215-L220.

10. A.Douhal, F. A.-R. (1993). Excited-state intramolecular proton transfer in jet-cooled 1-hydroxy-2-acetonaphthone. *Chem. Phys., 178*, 493.

11. A.J.G. Strandjord, P. B. (1983). Hydrogen/deuterium isotope effects on the excited-state proton transfer kinetics of 3-hydroxyflavone. *Chem. Phys., 98*, 21.

12. A.Pospieszczyk, P. H. (1980). Determination of low surface coverages of H2 and co by vacuum uv-resonance fluorescence spectroscopy of laser desorbed particles. *Journal of Nuclear Materials, 93-94*(1), 368-376.

13. A.U. Acuña, F.-G. A. (1991). Proton-transfer lasing from solid organic matrices. *Chemical Physics Letter, 187*, 98.

14. al., M. I.-V. (2012). Indigo - A Natural Pigment for High Performance Ambipolar Organic Field Effect Transistors and Circuits. *Adv. Mater., 24*, 375.

15. Aston, F. (1919). A positive ray spectrograph. *Philosophical Magazine and Journal of Science , 38*, 707-714.

16. B. A. Mamyrin, V. I. (1973). The mass-reflectron, a new nonmagnetic time-of-flight mass spectrometer with high resolution . *Sov. Phys.·JETP, 37*, 45.

17. Bell, R. (1980). Chapter 2. In *The Tunnel Effect in Chemistry.* New York: Chapmann Hall.

18. Boesl, U. (2000). Laser mass spectrometry for environmental and industrial chemical trace analysis. *Mass Spec., 35*(3), 289-304.

19. C. Janzen, D. S. (1999). Structure and vibrations of phenol(H2O)7,8 studied by infrared-ultraviolet and ultraviolet-ultraviolet double-resonance spectroscopy and ab initio theory. *J. Chem. Phys., 110*(20), 9898.

20. Campargue, R. (1970). Aerodynamic Separation Effect on Gas and Isotope Mixtures Induced by Invasion of the Free Jet Shock Wave Structure. *J. Chem. Phys., 52*(4), 1795.

21. D. Burgess Jr., P. C. (1986). Calculations of the surface temperature rise and desorption temperature in laser-induced thermal desorption. *Journal of Vacuum Science & Technology A, 4*(3), 1362.

22. D. H. Parker, S. J.-S. (1976). Multiphoton ionization spectrum of trans-hexatriene in the 6.2 eV region. *J. Chem. Phys., 65*(12), 5534.

23. D. Lubman, L. L. (1988). Pulsed laser desorption method for volatilizing thermally labile molecules for supersonic jet spectroscopy. *Review of Scientific Instruments, 59*(4), 557.

24. D. Menzel, R. G. (1964). Desorption from Metal Surfaces by Low-Energy Electrons. *J. Chem. Phys., 41*(11), 3311.

25. E. Nir, C. J. (2001). Guanine tautomerism revealed by UV–UV and IR–UV hole burning spectroscopy. *J. Chem. Phys., 115*, 4604 .

26. E. T. Mengesha, A. Z.-R. (2015). Spectroscopic Study of Jet-Cooled Deuterated Porphycenes: Unusual Isotopic Effects on Proton Tunneling. *J. Phys. Chem. B, 119*, 2193.

27. F. Hillenkamp, M. K. (1991). Matrix-Assisted Laser Desorption/Ionization Mass Spectrometry of Biopolymers. *Anal. Chem., 63*(24), 1193A–1203A.

28. G. B. Kistiakowsky, W. P. (1951). A High Intensity Source for the Molecular Beam. Part II. Experimental. *Review of Scientific Instruments , 22*(5), 333.

29. G. Meijer, M. S. (1990). Laser desorption jet-cooling of organic molecules. *Applied Physics B, 51*, 395–403.

30. G. Meijer, M. S. (1990). Laser desorption jet-cooling spectroscopy of para-amino benzoic acid monomer, dimer, and clusters. *J. Chem. Phys., 92*, 7625.

31. G. Petty, C. T. (1975). Nonlinear Resonant Photoionization in Molecular Iodine. *Phys. Rev. Lett. , 34*, 1207 .

32. G.J.Q.van der Peyl, J. P. (1982). Thermal aspects of laser desorption mass spectrometry. *International Journal of Mass Spectrometry and Ion Physics, 42*(1-2), 125-141.

33. G.Wedler, H. (1982). Laser induced thermal desorption of carbon monoxide from Fe(110) surfaces. *Surface Science, 121*(3), 464-486.

34. Gharanjig, M. H. (2015). Novel organic dyes based on thioindigo for dye-sensitized solar cells. *Dyes and Pigments , 123*, 147.

35. H. S. Katzenstein, S. S. (1955). New Time-of-Flight Mass Spectrometer. *Review of Scientific Instruments, 26*, 324.

36. Hilborn, R. C. (1982). Einstein coefficients, cross sections, f values, dipole moments, and all that. *American Journal of Physics, 50*, 982.

37. I. Iwakura, A. Y. (2010). Kinetic isotope effect on the proton-transfer in indigo carmine. *Chemical Physics Letters, 484*, 354.

38. I. Izumi, Y. A. (2009). Why is Indigo Photostable over Extremely Long Periods? *Chemistry Letters, 38*, 1020.

39. I. Izumi, Y. A. (2011). Transition State in a Prevented Proton Transfer Observed in Real Time. *Bull. Chem. Soc. Jpn. , 84*, 164.

40. J. L. Herek, S. P. (1992). Femtosecond real-time probing of reactions. IX. Hydrogen-atom transfer. *J. Chem. Phys., 97*, 9046.

41. J. Pina, D. S. (2017). Excited-State Proton Transfer in Indigo. *J. Phys. Chem. B, 121*, 2308.

42. J. R. Cable, M. J. (1987). Laser Desorption Molecular Beam Spectroscopy: The Electronic Spectra of Tryptophan Peptides in the Gas Phase. *J. Am. Chem. Soc, 109*, 6198-6199.

43. J. S. de Melo, R. R. (2006). Photophysics of an Indigo Derivative (Keto and Leuco Structures) with Singular Properties. *J. Phys. Chem. A, 110*, 13653.

44. J. S. de Melo, R. R. (2006). Spectral and Photophysical Studies of Substituted Indigo Derivatives in Their Keto Forms. *ChemPhysChem, 7*, 2303 .

45. J. Zhao, S. J. (2012). Excited state intramolecular proton transfer (ESIPT): from principal photophysics to the development of new chromophores and applications in fluorescent molecular probes and luminescent materials. *Phys. Chem. Chem. Phys., 14*, 8803.

46. J.B. Fenn, M. M. (1989). Electrospray Ionization for Mass Spectrometry of Large Biomolecules. *Science, 246*(4926), 64-71.

47. J.H. Hahn, R. Z. (1987). Subfemtomole Quantitation of Molecular Adsorbates by Two-Step Laser Mass Spectrometry. *J. Am. Chem. Soc, 109*, 2842-2843.

48. J.L.Brand, S. (1986). Effects of laser pulse characteristics and thermal desorption parameters on laser induced thermal desorption. *Surface Science, 167*(2-3), 341-362.

49. K. C. Ingham, M. A.-B. (1974). Photoinduced Double Proton Transfer in a Model Hydrogen Bonded Base Pair.1 Effects of Temperature and Deuterium Substitution. *Journal of the American Chemical Society, 96*, 1674.

50. K. J. Fallon, H. B. (2021). Indolonaphthyridine: A Versatile Chromophore for Organic Electronics Inspired by Natural Indigo Dye. *Acc. Chem. Res., 54*, 182.

51. K. Skonieczny, J. Y.-H. (2016). How To Reach Intense Luminescence for Compounds Capable of Excited-State Intramolecular Proton Transfer? *Chem.Eur.J, 22*, 7485.

52. K. Tanaka, H. W. (1988). Protein and polymer analyses up to m/z 100 000 by laser ionization time-of-flight mass spectrometry. *Rapid Communications in Mass Spectrometry, 2*, 151-153.

53. L. A. Chewter, M. S.-D. (1987). High resolution zero kinetic energy photoelectron spectroscopy of benzene and determination of the ionization potential. *J. Chem. Phys. , 86*(9), 4737 .

54. L. A. Huber, P. M. (2018). Photoisomerization of Mono-Arylated Indigo and Water-Induced Acceleration of Thermal cis-to-trans Isomerization. *ChemPhotoChem, 2*, 458.

55. L. Li, D. L. (1988). Analytical Jet Spectroscopy of Tyrosine and its Analogs Using a Pulsed Laser Desorption Volatilization Method. *Applied Spectroscopy, 42*(3), 418-424.

56. L. P. Levine, J. F. (1967). Gas Desorption Produced by a Giant Pulse Laser. *Journal of Applied Physics, 38*(1), 331.

57. Levy, D. (1980). Laser Spectroscopy of Cold Gas-Phase Molecules. *Ann. Rev. Phys. Chem, 31*, 197-225 .

58. Levy, D. (1981). The Spectroscopy of Very Cold Gases. *Science, 214*(4518), 263-269.

59. M. A. Manthrammel, I. S. (2019). Novel design and microelectronic analysis of highly stable Au/Indigo/n-Si photodiode for optoelectronic applications. *Solid State Sciences, 93*, 7.

60. M. A. Posthumus, P. G. (1978). Laser Desorption-Mass Spectrometry of Polar Nonvolatile Bio-Organic Molecules. *Analytical Chemistry, 50*(7), 985-991.

61. M. M. Wolff, W. E. (1953). A Pulsed Mass Spectrometer with Time Dispersion. *Review of Scientific Instruments, 24*, 616.

62. M. Moreno, J. M.-S. (2013). A theoretical study of the photochemistry of indigo in its neutral and dianionic (leucoindigo) forms. *Phys. Chem. Chem. Phys., 15*, 20236.

63. M. P. Callahan, Z. G. (2008). Resonant Two-Photon Ionization Mass Spectrometry of Jet-Cooled Phenolic Acids and Polyphenols. *Anal. Chem. , 80*, 2199-2203.

64. M. R. Haggmark, G. G. (2018). Evidence for competing proton-transfer and hydrogen-transfer reactions in the S1 state of indigo. *Chemical Physics*, 535-542.

65. P. Arrowsmith, M. S. (1988). Pulsed laser desorption near a jet orifice: Concentration profiles of entrained perylene vapor. *Applied Physics B, 46*, 165–173.

66. P. M. Johnson, M. R. (1975). Nonresonant multiphoton ionization spectroscopy: The four-photon ionization spectrum of nitric oxide. *J. Chem. Phys., 62*(6), 2500.

67. P. Voumard, R. Z. (1995). Spectroscopic Probe for Energy Transfer during Laser Desorption from Surfaces. *J. Phys. Chem., 99*(30), 11722–11727.

68. P.F. Barbara, P. K. (1989). Picosecond Kinetic and Vibrationally Resolved Spectroscopic Studies of Intramolecular Excited-State Hydrogen Atom Transfer. *J. Phys. Chem., 93*, 29.

69. P.P. Roy, J. S.-G. (2020). Solvent Mediated Excited State Proton Transfer in Indigo Carmine. *J. Phys. Chem. Lett. , 11*, 4156.

70. Q. Wang, Y. D. (2012). Highly selective DNA biosensor based on the long-range electron transfer of indigo carmine through DNA duplex. *Microchimica Acta , 179*, 273.

71. Qiao Zhan, S. J. (1997). Laser desorption substrate effects. *J Am Soc Mass Spectrom, 8*(5), 525–531.

72. R. B. Van Breemen, M. R. (1983). Time-resolved laser desorption mass spectrometry. I. Desorption of preformed ions. *International Journal of Mass Spectrometry and Ion Physics, 49*(1), 35-50.

73. R. E. Smalley, L. W. (1975). The fluorescence excitation spectrum of rotationally cooled NO2. *J. Chem. Phys. , 63*(11), 4977.

74. R. E. Smalley, L. W. (1977). Molecular optical spectroscopy with supersonic beams and jets. *Acc. Chem. Res., 10*(4), 139–145.

75. R. H. Page, Y. R. (1988). Local modes of benzene and benzene dimer, studied by infrared–ultraviolet double resonance in a supersonic beam. *J. Chem. Phys. , 88*(8), 4621.

76. R. J. Wenzel, U. M. (2005). Analysis of Megadalton Ions Using Cryodetection MALDI Time-of-Flight Mass Spectrometry. *Anal. Chem., 77*, 4329–4337.

77. R. R. Cavanagh, D. S. (1993). Dynamics of Nonthermal Reactions: Femtosecond Surface Chemistry. *J. Phys. Chem., 97*, 786-798.

78. R.B., H. (1987). Pulsed-laser-induced desorption studies of the kinetics of surface reactions. *J. Phys. Chem., 91*(5), 1007–1015.

79. R.N.Zare, R. (1987). Mechanism for bond-selective processes in laser desorption. *Chemical Physics Letters, 136*(6), 593-599.

80. R.R. Lucchese, J. C. (1984). Laser induced thermal desorption from surfaces. *J. Chem. Phys. , 81*(12), 6313.

81. S. Ameer-Beg, S. M. (2001). Ultrafast Measurements of Excited State Intramolecular Proton Transfer (ESIPT) in Room Temperature Solutions of 3-Hydroxyflavone and Derivatives. *J. Phys. Chem. A , 105*, 3709–3718.

82. S. Yamazaki, A. L. (2011). Molecular mechanisms of the photostability of indigo. *Phys. Chem. Chem. Phys., 13*, 1618.

83. S.Braun. (2001). In *Spectral Analysis, Classical Methods* (Vols. 1-3, pp. 1208-1223).

84. S.J. Formosinho, L. A. (1992). Excited-state proton transfer reactions II. Intramolecular reactions. *J. Photochem. Photobiol. A: Chem., 75*, 21-48.

85. Scheiner, S. (2000). Calculation of isotope effects from first principles. *Biochimica et Biophysica Acta, 1458*, 28.

86. Stephens, W. (1946). A Pulsed Mass Spectrometer with Time Dispersion. *Phys. Rev., 69*, 11–12.

87. T. Mutai, H. T. (2008). Switching of Polymorph-Dependent ESIPT Luminescence of an Imidazo[1,2-a]pyridine Derivative. *Angew. Chem. Int. Ed., 47*, 9522.

88. U.Boesl, H. E. (1981). Multi-photon ionization in the mass spectrometry of polyatomic molecules: Cross sections. *Chemical Physics, 55*(2), 193-204.

89. V. Luxamia, S. K. (2008). Molecular half-subtractor based on 3,3′-bis(1H-benzimidazolyl-2-yl)[1,1′]binaphthalenyl-2,2′-diol. *New J. Chem., 32*, 2074.

90. W. C. Wiley, I. H. (1955). Time-of-Flight Mass Spectrometer with Improved Resolution. *Review of Scientific Instruments , 26*, 1150.

91. Waluk, J. (2008). Proton or Hydrogen Transfer? Charge distribution analysis. *Polish Journal of Chemistry, 82*, 947.

92. Weller, A. (1952). *Elektrochemie, 56*, 662.

93. Wiza, J. (1979). Microchannel plate detectors. *Nuclear Instruments and Methods, 162*, 587-601.

94. Y. Nagasawa, R. T. (2004). The effect of hydrogen-bonding on the ultrafast electronic deactivation dynamics of indigo carmine. *Phys. Chem. Chem. Phys., 6*, 5370.

95. Z. Wang, K. S. (2017). Development of indigo-based nonvolatile write-once-read-many-times memory device. *Materials Letters, 206*, 128.

96. Zewail, A. H. (2000). Femtochemistry: Atomic-Scale Dynamics of the Chemical Bond Using Ultrafast Lasers (Nobel Lecture). *Angew. Chem. Int. Ed., 29*, 2586.

## Appendix

**Table 2. Summary of discussed kinetic isotope studies of indigo and its derivatives**

| Year/Author/Citation | Species | Method | Result |
|---|---|---|---|
| 2004/ Nagasawa/28 | Indigo carmine | Solution phase: femtosecond transient absorption spectroscopy and steady-state Raman spectroscopy | Slower recovery upon deuteration |
| 2006/de Melo/29 | Indigo and derivatives | Solution phase: emission spectra, quantum yields of fluorescence, singlet oxygen formation, fluorescence lifetimes | biexponential decay |
| 2006/de Melo/30 | Indigo/ Cibalackrot | Solution phase: absorption spectra, fluorescence, pulse radiolysis | Reverse isotope effect: $k_H/k_D < 1$ |
| 2004/Iwakura/31 | Indigodisulfonate salt | Solution phase: fs pump probe time-resolved difference transmittance | Isotope effect: $k_H/k_D = 1.7$ |
| 2010/Iwakura/32 | Indigo carmine | Solution phase: fs pump probe time-resolved difference transmittance | Isotope effect: $k_H/k_D = 1.5$ |
| 2020/Roy/34 | Indigo carmine | Solution phase: visible pump–infrared probe and two-dimensional electronic–vibrational (2DEV) spectroscopy | Faster decay upon deuteration |